Supporting Information

Noria and its derivatives as hosts for chemically and thermally robust Type II Porous Liquids

Francesca M. Alexander,[a] Sergio F. Fonrouge,[b] José L. Borioni,[b] Mario G. del Pópolo,[b] Peter N. Horton,[c] Simon J. Coles, [c] Benjamin P. Hutchings,[a] Deborah E. Crawford[d] and Stuart L. James[a*]

[a] School of Chemistry and Chemical Engineering, Queen's University Belfast, David Keir Building Stranmillis Road, Belfast, BT7 1NN, UK

[b] ICB-CONICET and Facultad de Ciencias Exactas y Naturales, Universidad Nacional de Cuyo, Padre Jorge Contreras 1300, Mendoza, CP5500, Argentina

[c] EPSRC National Crystallography Service, School of Chemistry, Faculty of Engineering and Physical Sciences, University of Southampton, Southampton, SO17 1BJ, UK

[d] School of Chemistry and Bioscience, University of Bradford, Richmond Road, Bradford, BD7 1DP, UK

*Corresponding author: S.James@qub.ac.uk

Table of Contents

Mass spectrumMass spectrumMass spectrumMass spectrum

List of Schemes

List of Figures

List of Tables

S1. General synthetic & Analytical methods

Materials:

All chemicals were purchased from Fluorochem, Alfa Aesar or Sigma-Aldrich and used as received. Solvents were reagent or High performance liquid chromatography (HPLC) grade purchased from Fisher Scientific or Sigma-Aldrich (these were used as received unless specified), with the exception of 15-crown-5, which was purchased from Fluorochem and dried over calcium hydride before use.

Synthesis:

All reactions were stirred magnetically using Teflon-coated stirring bars. Where heating was required, the reactions were warmed using a stirrer hotplate with the stated temperature being measured externally to the reaction flask with an attached probe. Removal of solvents was done using a rotary evaporator.

Nuclear Magnetic Resonance (NMR) spectra:

Proton (^{1}H) Nuclear magnetic resonance (NMR) spectra were recorded using an internal deuterium lock for the residual protons in deuterated dimethyl sulfoxide (d_6-DMSO) (δ = 2.50 ppm) at ambient probe temperature using a Bruker 600 (600 MHz) instrument. NMR data are presented as follows: chemical shift, peak multiplicity (s = singlet, d = doublet, t = triplet, q = quartet, m = multiplet and br = broad), integration and assignment. Chemical shifts are expressed in ppm on a δ scale relative to δd_6-DMSO (2.50 ppm). Assignments were determined either on the basis of unambiguous chemical shift or coupling patterns or by analogy to fully interpreted spectra for structurally related compounds. Carbon (^{13}C) NMR spectra were recorded using an internal deuterium lock using d_6-DMSO (δ = 39.52 ppm) at ambient probe temperatures using a Bruker 600 (600 MHz) instrument.

Mass Spectrometry (MS):

MS spectra were obtained from the National Mass Spectrometry Facility (NMSF) at Swansea University, UK, using:

- Matrix-assisted laser desorption/ionization time-of-flight (MALDI-TOF) (Bruker ultrafleXtreme or Applied Biosystems Voyager DE-STR) in positive-reflection mode using a solvent-free preparation with trans-2-[3-(4-tert-Butylphenyl)-2-methyl-2-propenylidene]malononitrile (DCTB) matrix and/or without sodium acetate (NaOAc) additive, or
- Positive nano-electrospray ionization (nanoESI) on a Thermo Scientific LTQ Oribitrap XL instrument, with an Advion NanoMate Triversa source.

TGA:

Thermogravimetric Analyses (TGA) were measured by Queen's University Ionic Liquid Laboratories (QUILL) using a TGA Q5000 V3.17 Build 265 instrument. The samples were heated at the rate of 10°C/min to 500°C in sealed aluminium pan under a nitrogen flow. All solid materials were desolvated by heating to between 80 and 100°C in a vacuum oven overnight prior to TGA analysis.

Viscosity:

Viscosity measurements were carried out using a SV-1A 0.3 ~ 1000 mPa·s Tuning ForkVibroViscometer.

Brunauer–Emmett–Teller (BET):

BET measurements were carried out using a Quantachrome NOVA 4200e Surface Area and Pore Size Analyzer.

X-ray Crystallography:

Single crystal data was obtained from the national crystallography service (ncs) (See section S6).

S2. Synthesis & Characterisation

S2.1 Synthesis of Product 1 (Crude Noria)

Product 1 was prepared according to the following scheme:
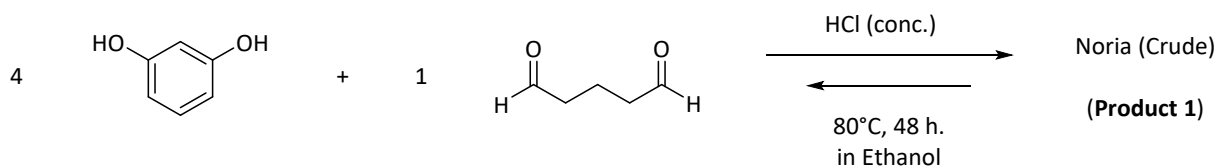
Scheme S1. Crude Noria Synthesis.

Crude Noria, **Product 1**, was synthesised using an adapted previously reported literature procedure.[1] To a round bottomed flask (RBF) resorcinol (44.0 g, 399.6 mmol), ethanol (91 mL) and concentrated (conc.) hydrochloric (HCl) acid (60 mL) were added and agitated for 10 min. Glutyraldehyde (1,5-pentanedial, 50% in H_2O) (19.9 g, 99.4 mmol) was added over 15 minutes and the reaction mixture was refluxed at 80°C for 48h. The reaction mixture was cooled to room temperature (rt) and poured into methanol (MeOH) (500 mL). The suspension was centrifuged (20 min, 4000 RPM), washed with diethyl ether (Et_2O) (400 mL) and centrifuged again (20 min, 4000 RPM) to afford **Product 1** as a yellow solid. This crude product was dried in vacuum at 80°C overnight (crude yield 25.9 g, 92%).
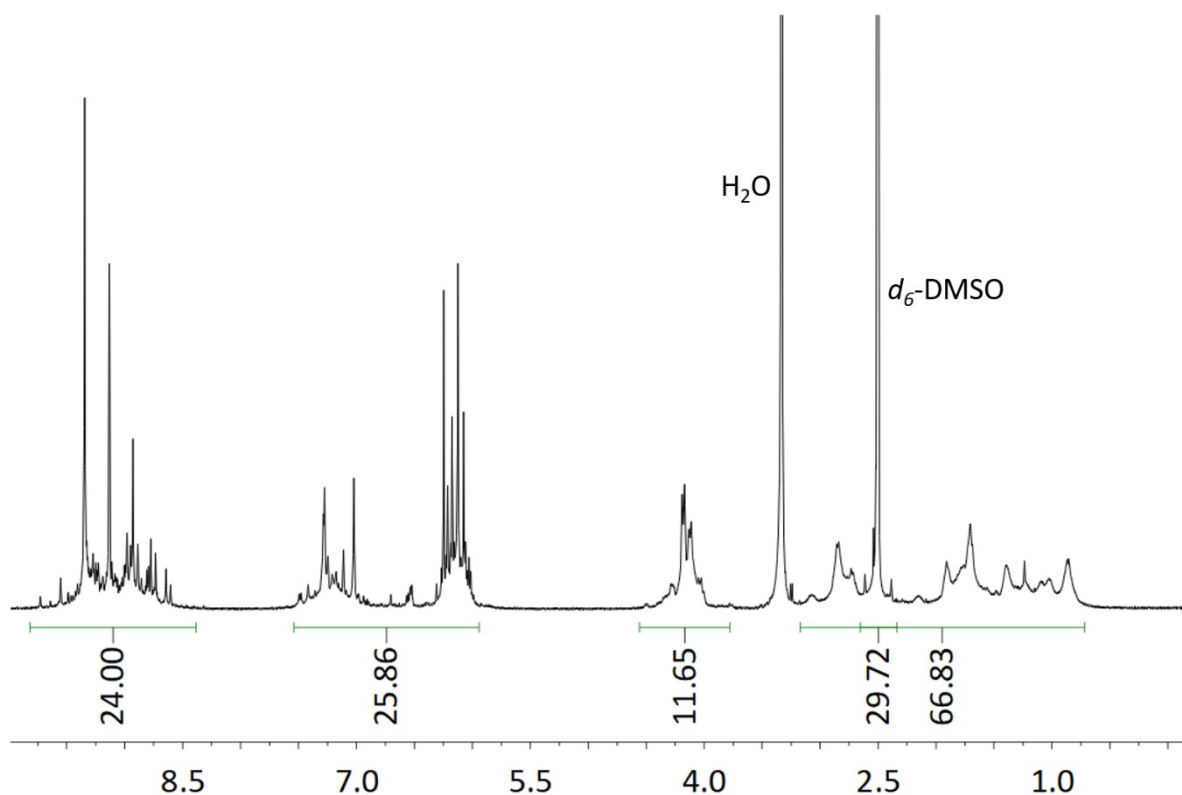
Figure S1. ^{1}H NMR spectrum of **Product 1.**

^{1}H NMR (600 MHz, d_6-DMSO): δ(ppm) 0.72-3.18 ppm (m, 36H, -CH$_2$CH$_2$CH$_2$- (N.B. overlaps with solvent)), 3.77-4.56 ppm (m, 12H, >CH-), 5.94-7.55 ppm (m, 26H, Ar-H), 8.39-9.81 ppm (m, 24H, -OH). The ^{1}H NMR spectrum was consistent with that reported by Kudo et al..[1]

Note **Product 1** was found to be a mixture of species and therefore no compound has been shown. The assignment above is based on previously reported ^{1}H NMR data reported by Kudo et al..[1]

S2.1.1 Mass spectrum for Product 1

MALDI-TOF:

[M]$^{+•}$, theoretical: 1704.6 m/z, Observed: 1704.8 m/z (weak)
[M + Na]$^+$, theoretical: 1727.6 m/z, Observed: 1727.8 m/z
[M + K]$^+$, theoretical: 1743.6 m/z, Observed: 1743.8 m/z
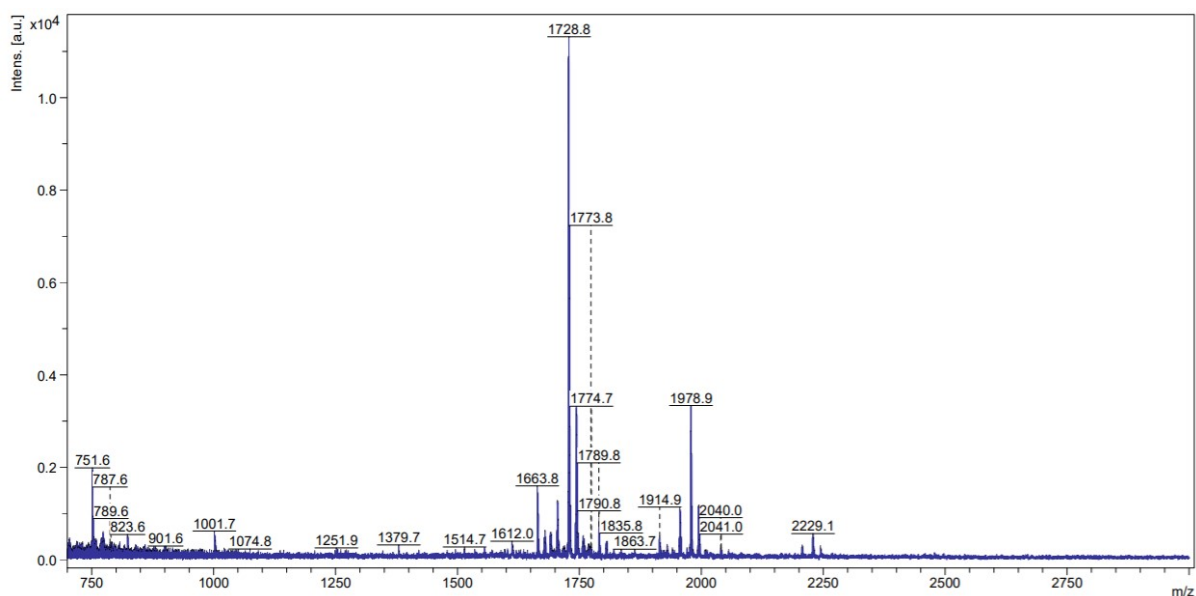
Figure S2. Product 1 mass spectrum (MALDI (ultrafleXtreme)).

S2.1.2 Thermal Gravimetric Analysis (TGA) for Product 1

Decomposition temperature = 314°C.
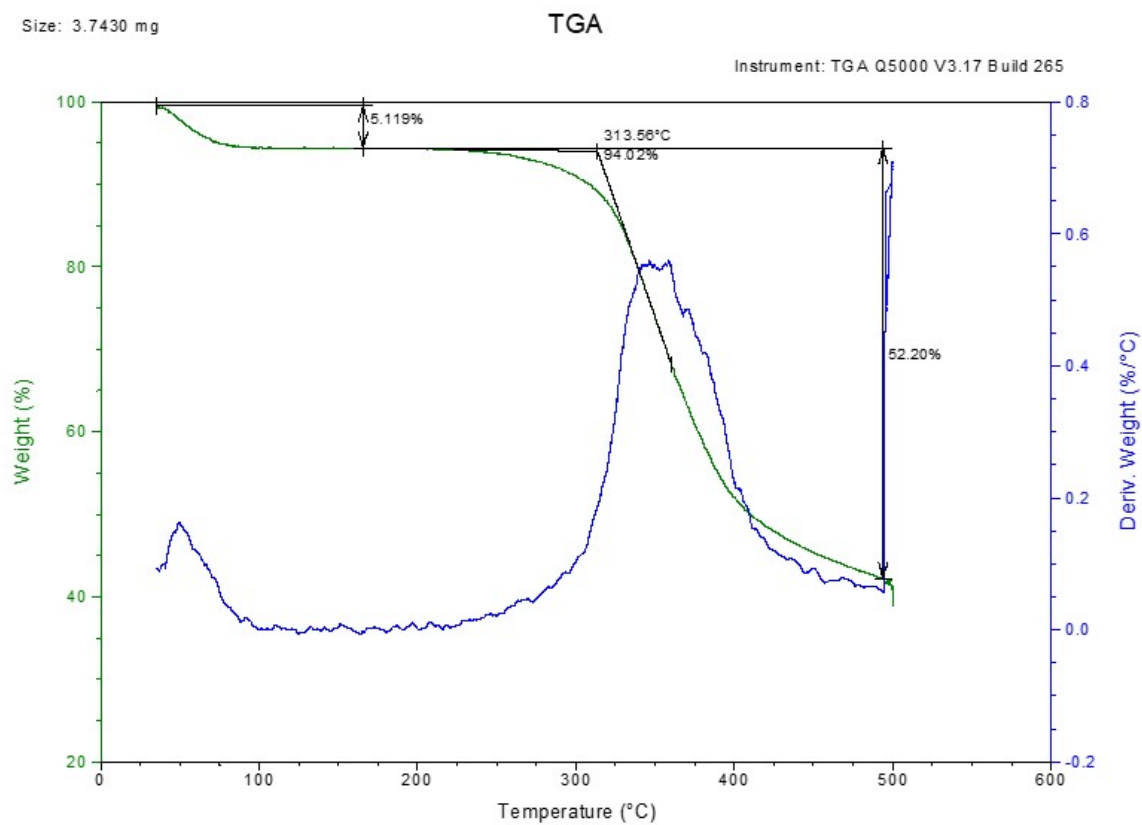
Figure S3. TGA of **Product 1.**

S2.2 Isolation of Product 2, R3
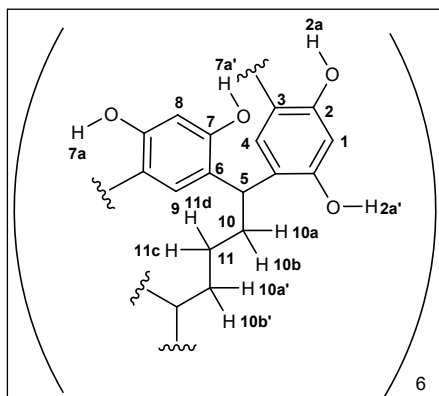
Product 1 (0.6 g) was recrystallised from DMSO with cold MeOH (21 mL and 7.8 mL respectively). The suspension was then centrifuged (10 min, 4000 RPM) and washed with Et$_2$O (70 mL) to afford **Product 2** as a pale cream solid. The product was dried in vacuum at 80°C overnight (yield 0.1319 g, 22%).

It should be noted that the structural diagram here is simplified and does not show the stereochemistry of R3; H5 and H10a/a' are mutually *anti*, as are (H10a/a' and H11c) and (H10b/b' and H11d). The rim and side resorcinol units cannot be distinguished and therefore they have not been specified in the following assignment. **Figure S4** shows the full structure of R3.
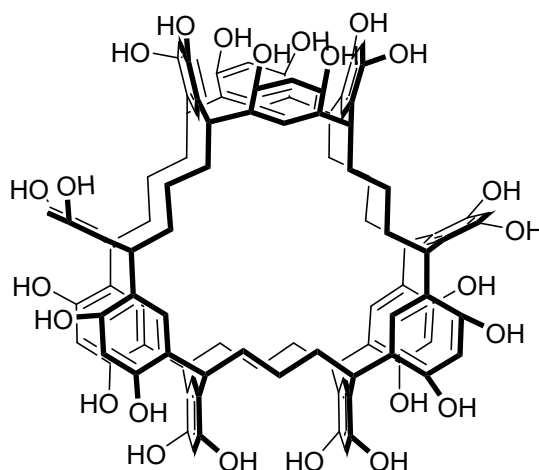
Figure S4. Full Structure of R3**.**
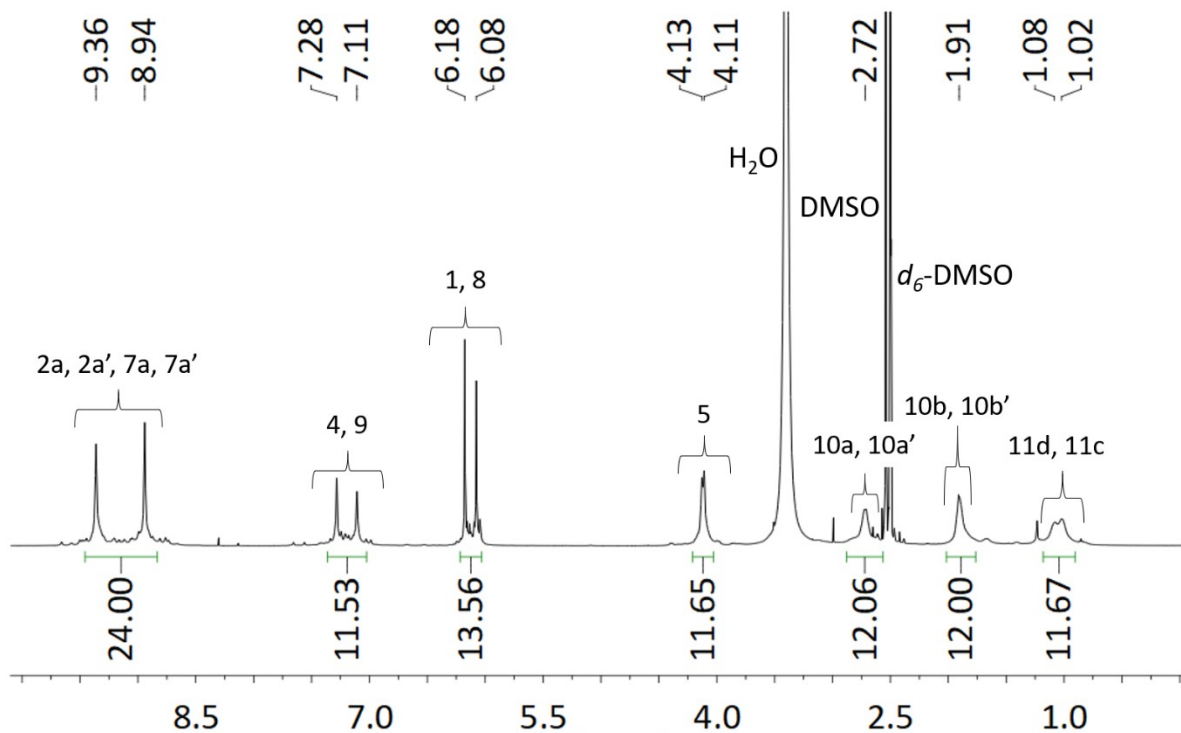
Figure S5. ^{1}H NMR spectrum of **Product 2.**

^{1}H NMR (600 MHz, d_6-DMSO): δH(ppm) 1.02-1.08 ppm (br, 12H, -CH$_2$-, H$_{11d}$ and H$_{11c}$), 1.91 ppm (br, 12H, -CH$_2$-, H$_{10b}$, H$_{10b'}$), 2.72 ppm (br, 12H, -CH$_2$-, H$_{10a}$, H$_{10a'}$), 4.12 ppm (m, 12H, >CH-, H$_5$), 6.08-6.18 ppm (two s, 14H (should be 12H), Ar-H, H$_1$, H$_8$), 7.11-7.28 ppm (two s, 12H, Ar-H, H$_4$, H$_9$), 8.94-9.36 ppm (two s, 24H, -OH, H$_{2a}$, H$_{2a'}$, H$_{7a}$, H$_{7a'}$)
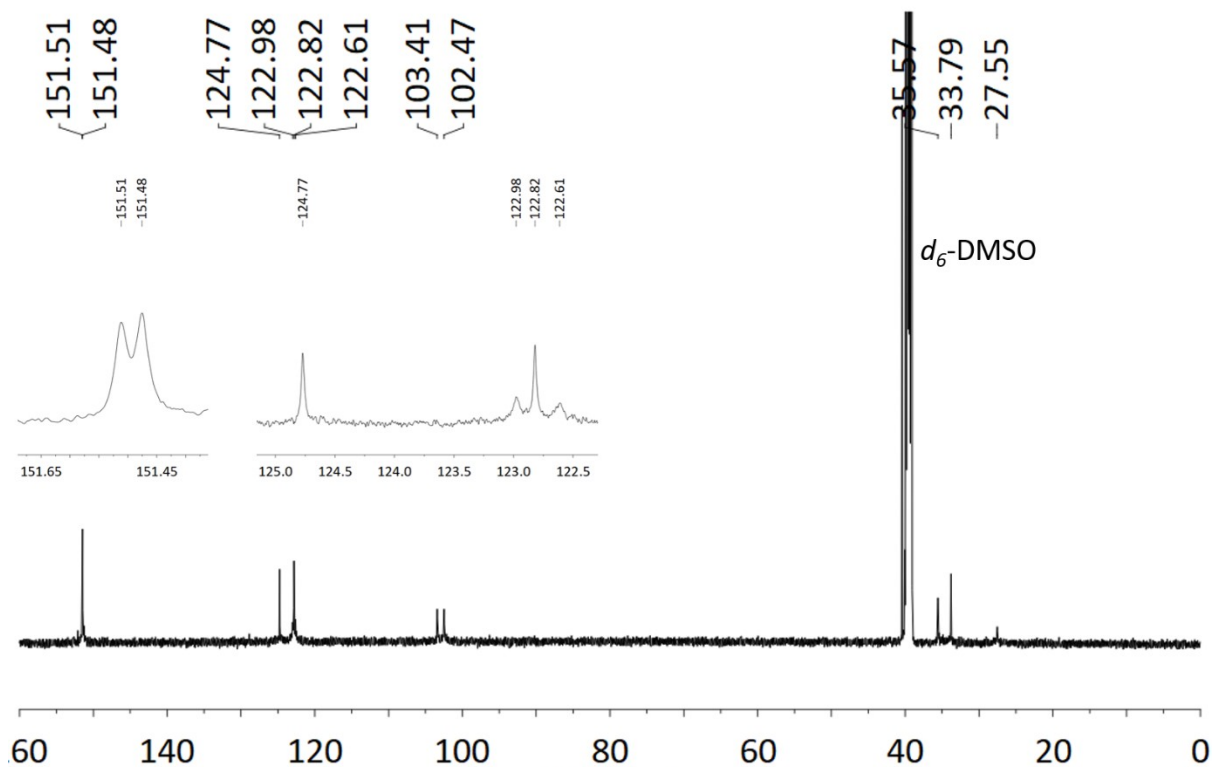
Figure S6. ¹³C NMR spectrum of **Product 2.**

¹³C NMR (600 MHz, *d*₆-DMSO): δC(ppm) 27.6, 33.8, 35.6, 102.5, 103.4, 122.6, 122.8, 123.0, 124.8, 151.48, 151.51
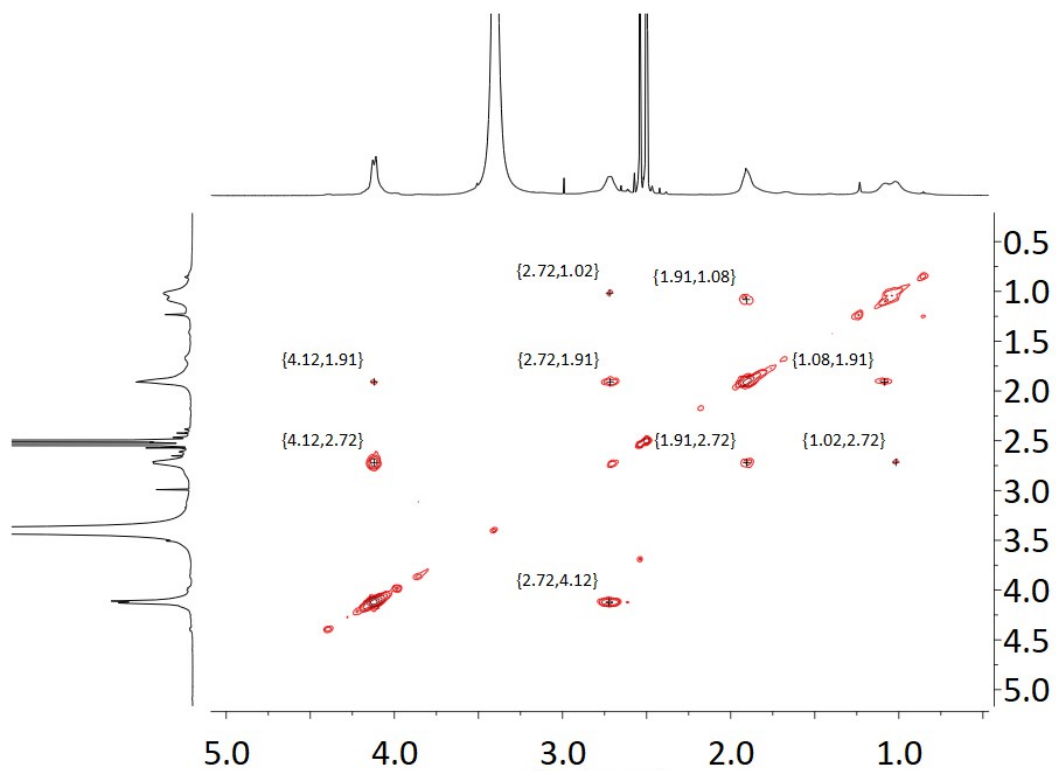
Figure S7. ¹H-¹H Correlation Spectroscopy (COSY) spectrum of **Product 2.**
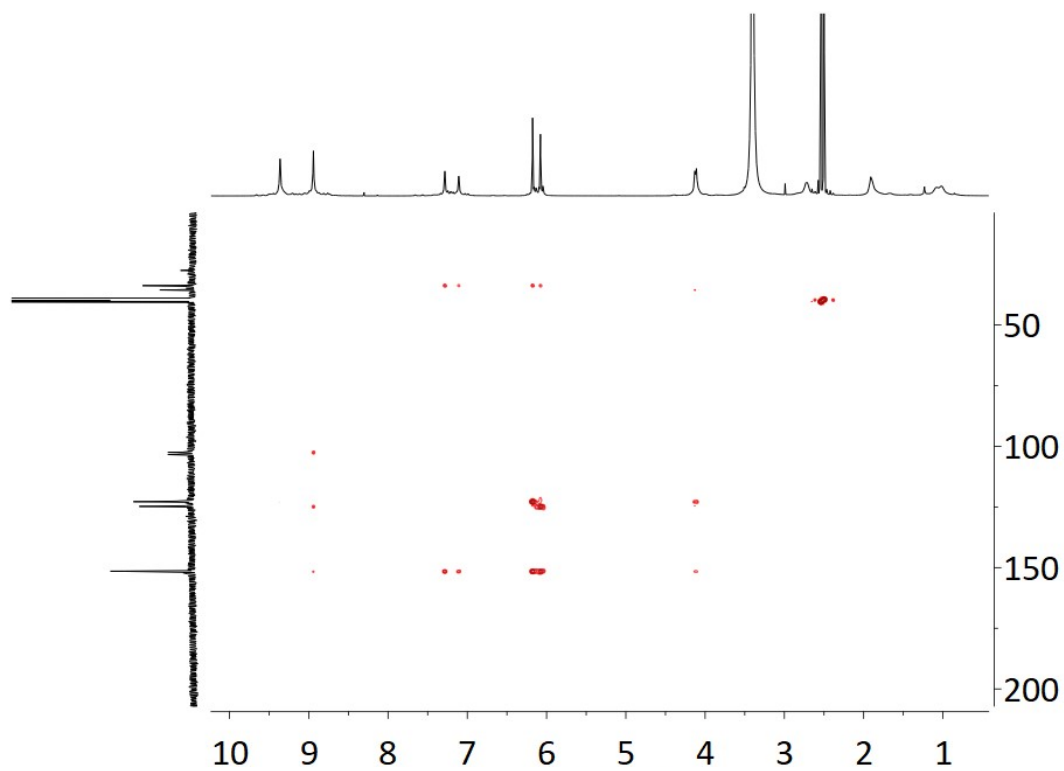
Figure S8. Heteronuclear Multiple Bond Correlation (HMBC) spectrum of **Product 2.**
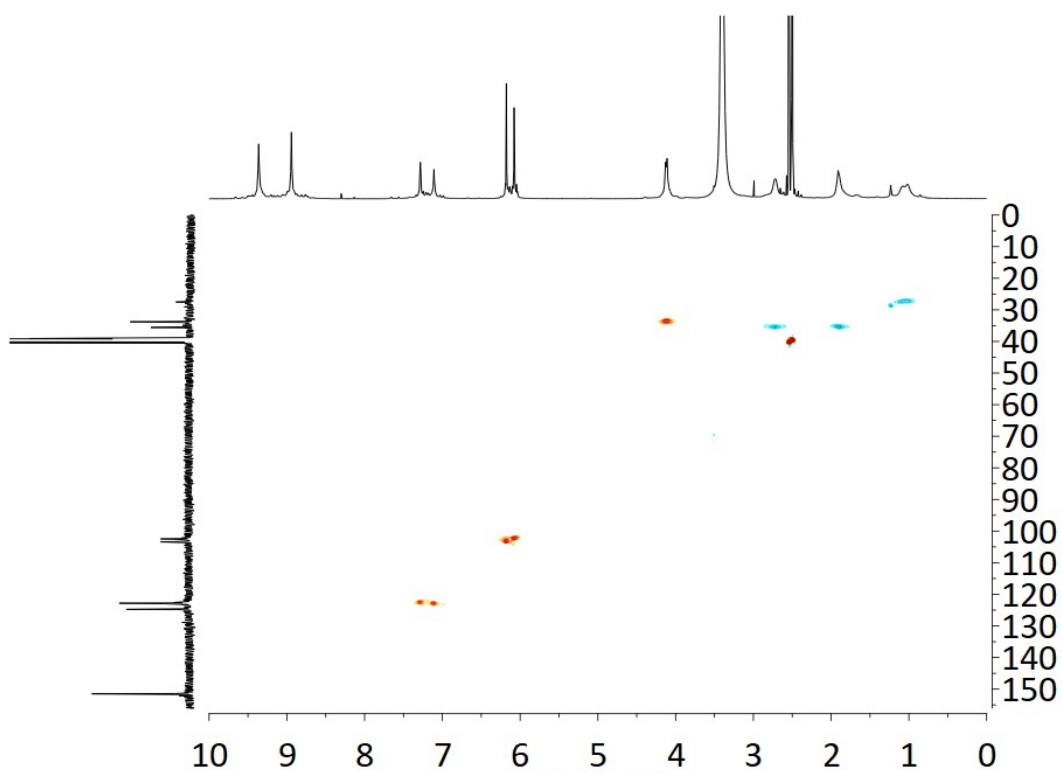
Figure S9. Heteronuclear Single Quantum Coherence (HSQC) spectrum of **Product 2.**
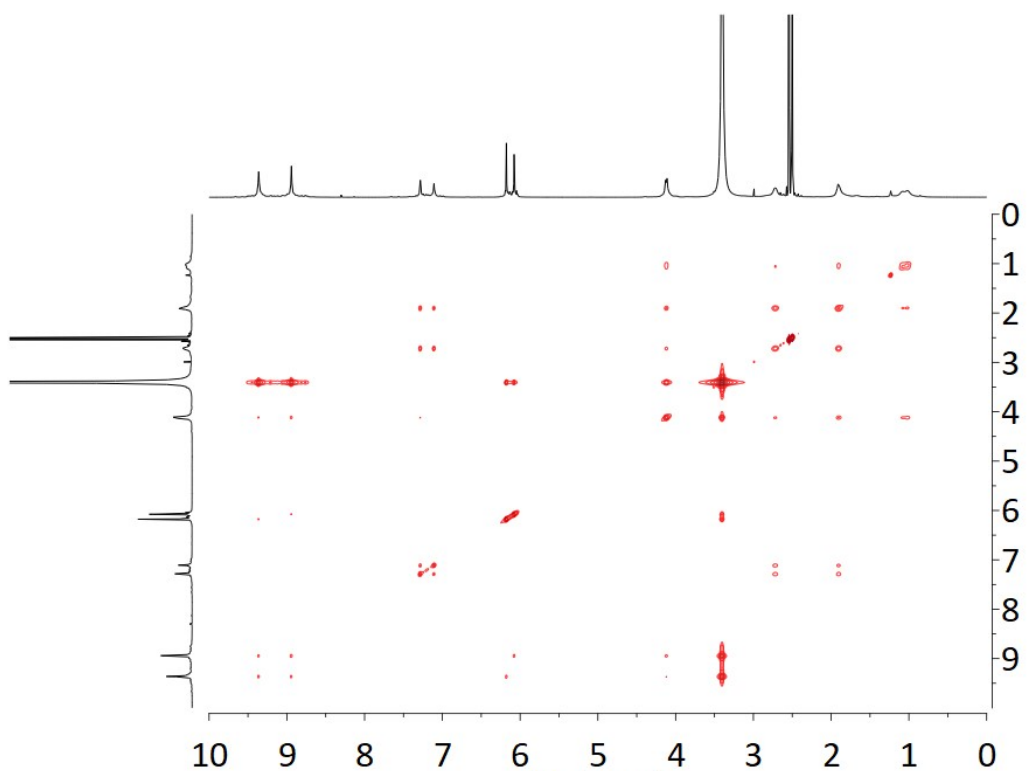
Figure S10. Nuclear Overhauser Effect Spectroscopy (NOSEY) spectrum of **Product 2.**

S2.2.1 Mass spectrum for Product 2

MALDI-TOF:

[M]$^{+\bullet}$, theoretical: 1704.6 m/z, Observed: 1704.7 m/z
[M + Na]$^+$, theoretical: 1727.6 m/z, Observed: 1727.7 m/z
[M + K]$^+$, theoretical: 1743.6 m/z, Observed: 1743.6 m/z
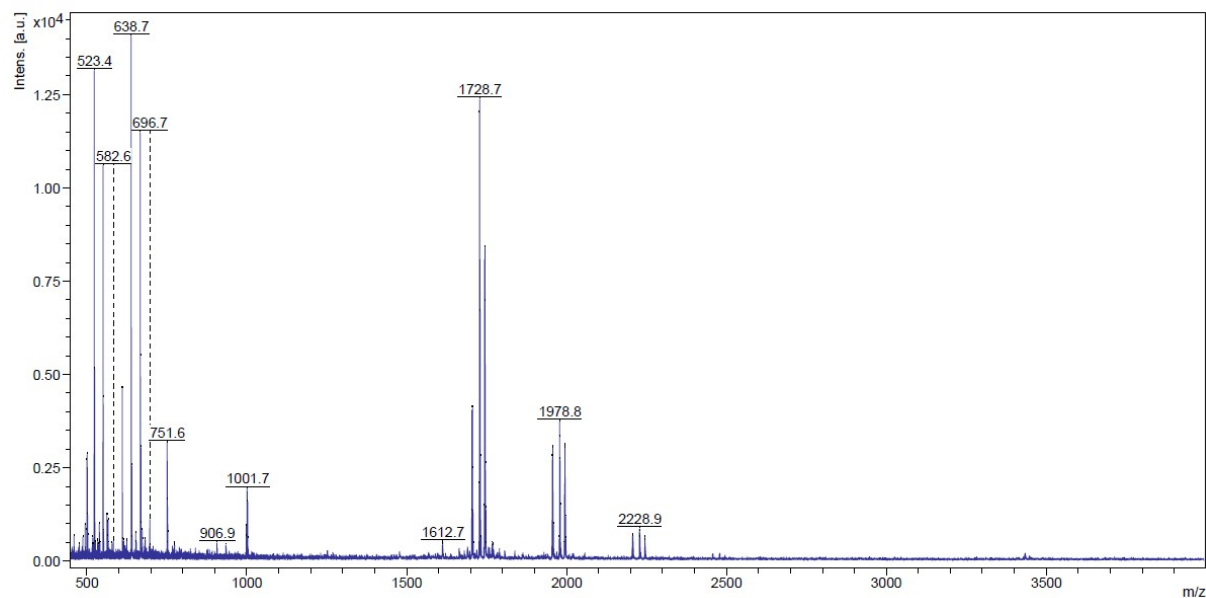
Figure S11. Product 2 mass spectrum (MALDI (ultrafleXtreme))**.**

The higher mass species (an increase of 250 mass units) may be attributed to complexes of DCTB (DCTB = trans-2-[3-(4-tert-Butylphenyl)-2-methyl-2-propenylidene]malononitrile matrix) with **Product 2**, [M+Na+DCTB]$^+$ and [M + Na + 2DCTB]$^+$ i.e., DCTB may be able to reside inside the cavity of R3 (**Figure S12** shows DCTB structure).
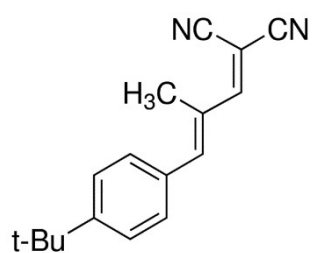
Figure S12. Structure of DCTB.

S2.2.2 TGA for Product 2

Decomposition temperature = 356°C.
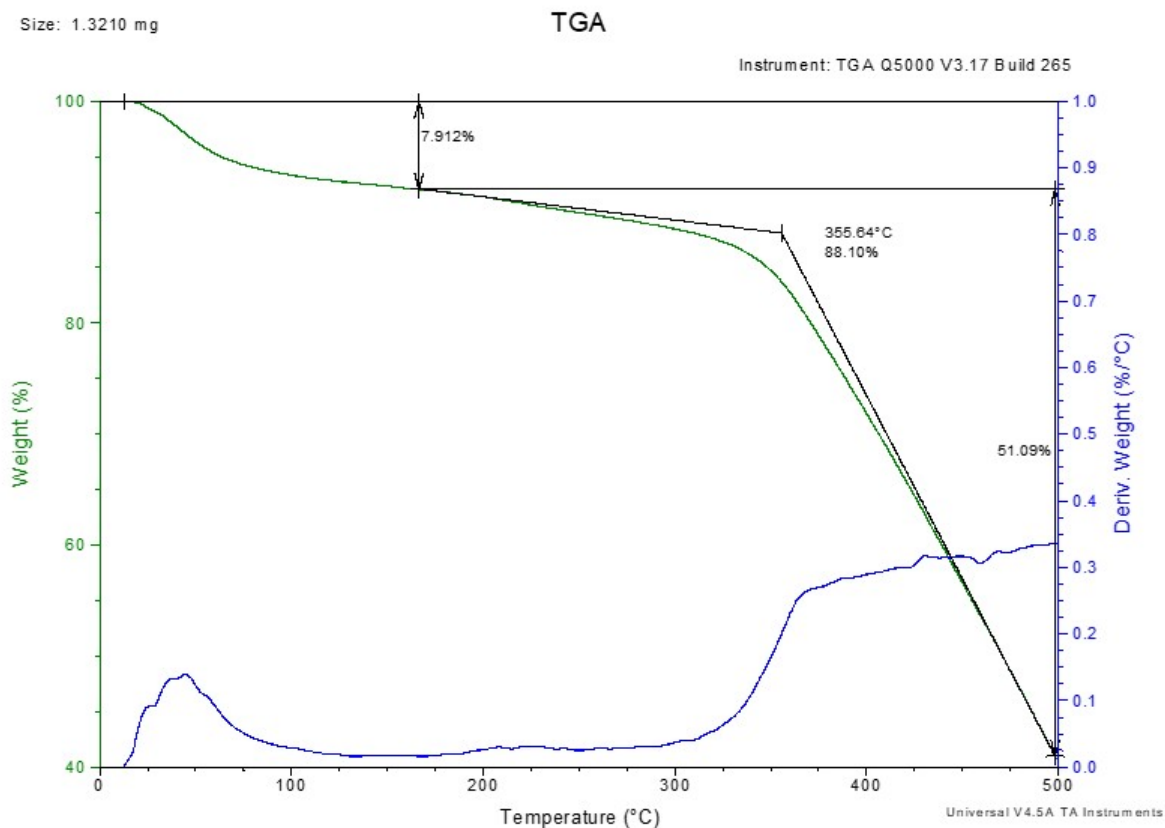
Figure S13. TGA of **Product 2**.

S2.3 Single Crystal Growth of Product 3
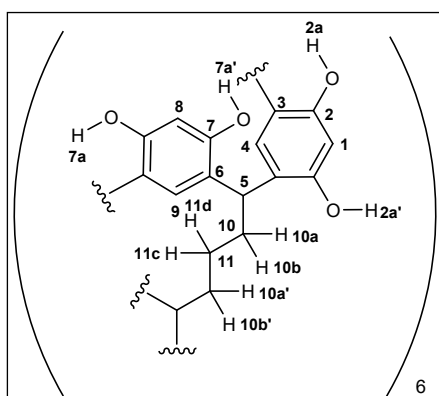
Product 2 was washed with dimethylformamide (DMF) and then dissolved in a minimum of DMSO and added to a 1 mL vial which was capped with a punctured lid. This was placed in a 5 mL capped vial with tetrahydrofuran (THF) as the anti-solvent which was allowed to diffuse over the course of several weeks. Single colourless plate crystals of R3 (**Product 3**) were obtained. Refer to section S6.
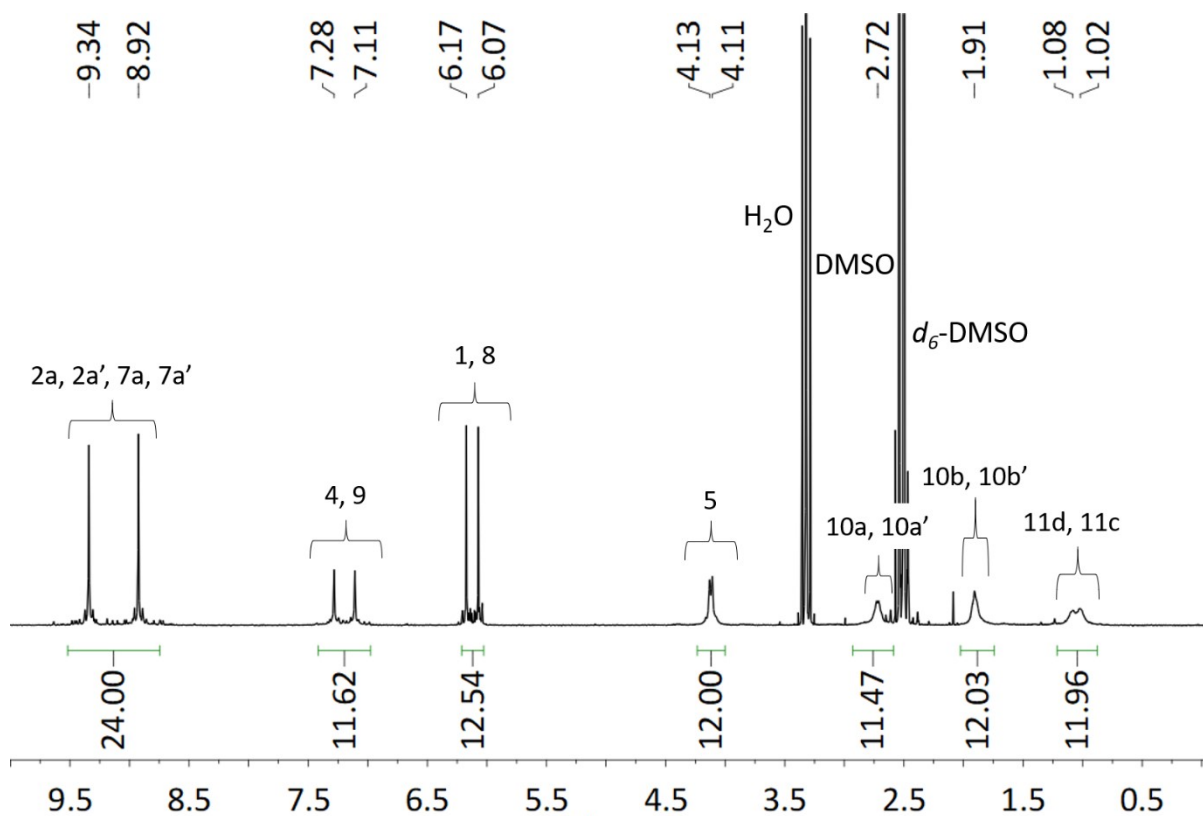
Figure S14. ^{1}H NMR spectrum of **Product 3.**

^{1}**H NMR (600 MHz, d_6-DMSO)**: δH(ppm) 1.02-1.08 ppm (br, 12H, -CH$_2$-, H$_{11d}$ and H$_{11c}$), 1.91 ppm (br, 12H, -CH$_2$-, H$_{10b}$, H$_{10b'}$), 2.72 ppm (br, 12H, -CH$_2$-, H$_{10a}$, H$_{10a'}$), 4.12 ppm (m, 12H, >CH-, H$_5$), 6.07-6.17 ppm (two s, 13H (should be 12H), Ar-H, H$_1$, H$_8$), 7.11-7.28 ppm (two s, 12H, Ar-H, H$_4$, H$_9$), 8.92-9.34 ppm (two s, 24H, -OH, H$_{2a}$, H$_{2a'}$, H$_{7a}$, H$_{7a'}$)

S2.4 Product 4

Soxhlet extraction was performed using 8 g of **Product 1** (crude Noria). After 9 days of the Soxhlet extraction the remaining material in the porous thimble was recovered and dried in vacuum at 80°C overnight to afford **Product 4** as a yellow solid (Crude yield 6.95 g).

Note that similarly to **Product 1**, **Product 4** is a mixture of species.
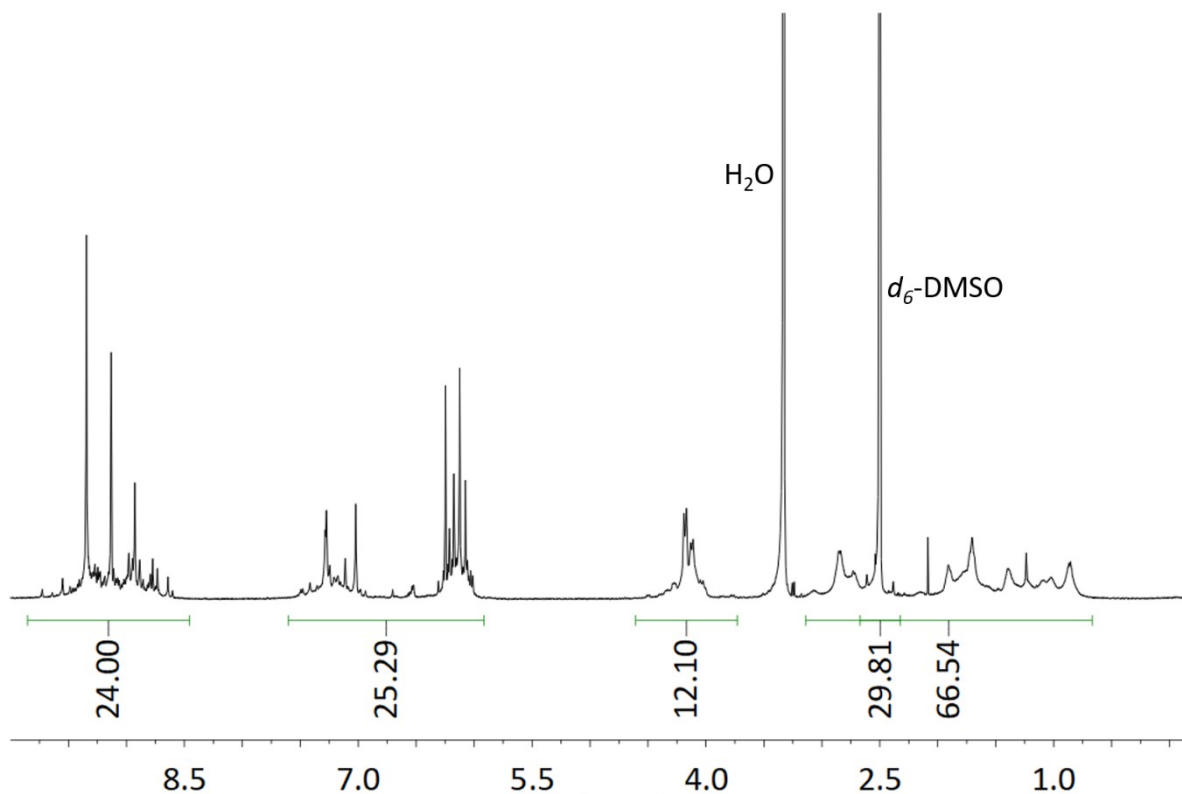
Figure S15. ^{1}H NMR spectrum of **Product 4**.

S2.5 Isolation of Product 5
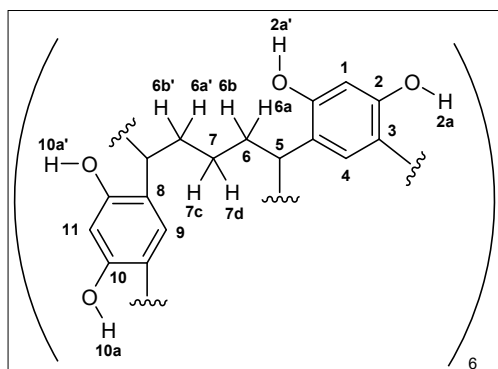
Soxhlet extraction was performed using 8 g of **Product 1** (crude Noria). **Product 5** was extracted under reflux at 80°C with 400 mL of MeOH for 9 days. After cooling to rt the MeOH solution was centrifuged (20 min, 4000 RPM), washed with Et$_2$O (400 mL) and centrifuged again (20 min, 4000 RPM) to afford **Product 5** as a pale cream solid which was dried in vacuum at 80°C overnight (yield 0.20 g, 2.5%).

It should be noted that the structural diagram here is simplified and does not show the stereochemistry of Noria; H5 and H6a/a' are mutually *anti*, as are (H6a/a' and H7c) and (H6b/b' and H7d). The rim and side resorcinol units cannot be distinguished and therefore they have not been specified in the following assignment.
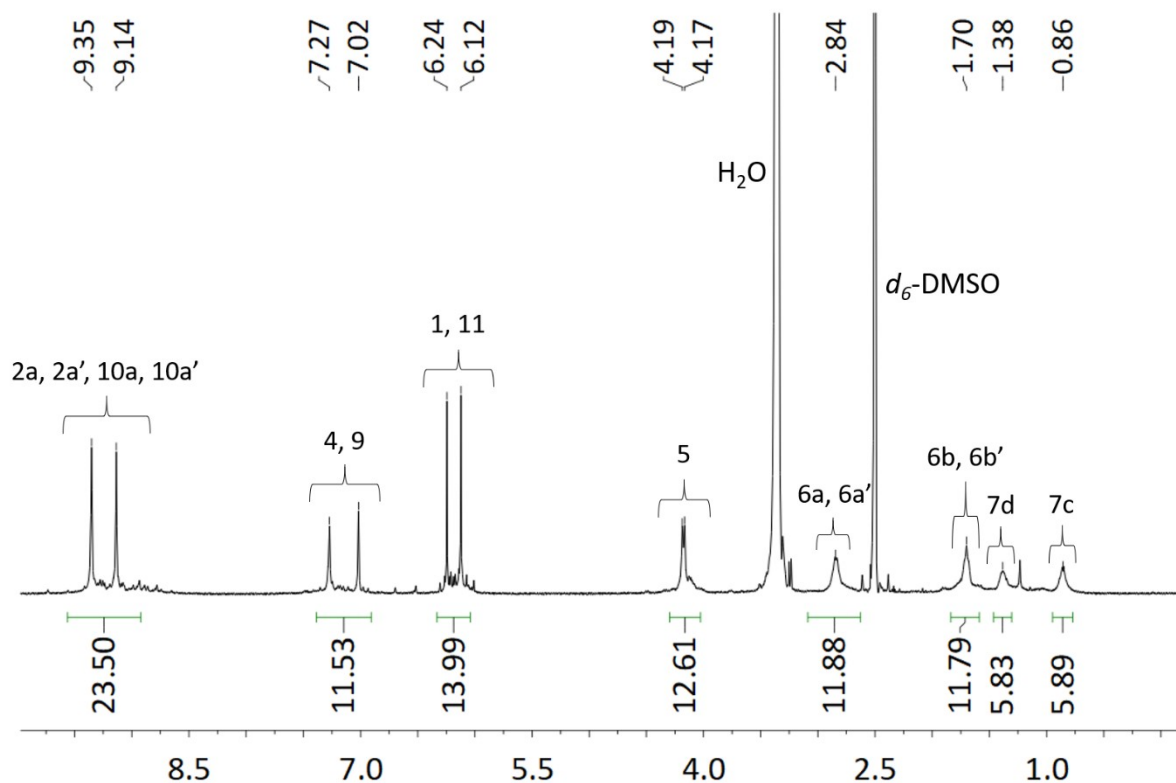
Figure S16. ^{1}H NMR spectrum of **Product 5.**

^{1}H NMR (600 MHz, d_6-DMSO): δH(ppm) 0.86 ppm (br, 6H, H$_{7c}$), 1.38 ppm (br, 6H, H$_{7d}$), 1.70 ppm (br, 12H, -CH$_2$-, H$_{6b}$, H$_{6b'}$), 2.84 ppm (br, 12H, -CH$_2$-, H$_{6a}$, H$_{6a'}$), 4.18 ppm (m, 13H (should be 12H), >CH-, H$_5$), 6.12-6.24 ppm (m, 14H (should be 12H), Ar-H, H$_1$, H$_{11}$), 7.02-7.27 ppm (12H, Ar-H, H$_4$, H$_9$), 9.14-9.35 ppm (m, 24H, -OH, H$_{2a}$, H$_{2a'}$, H$_{10a}$, H$_{10a'}$)
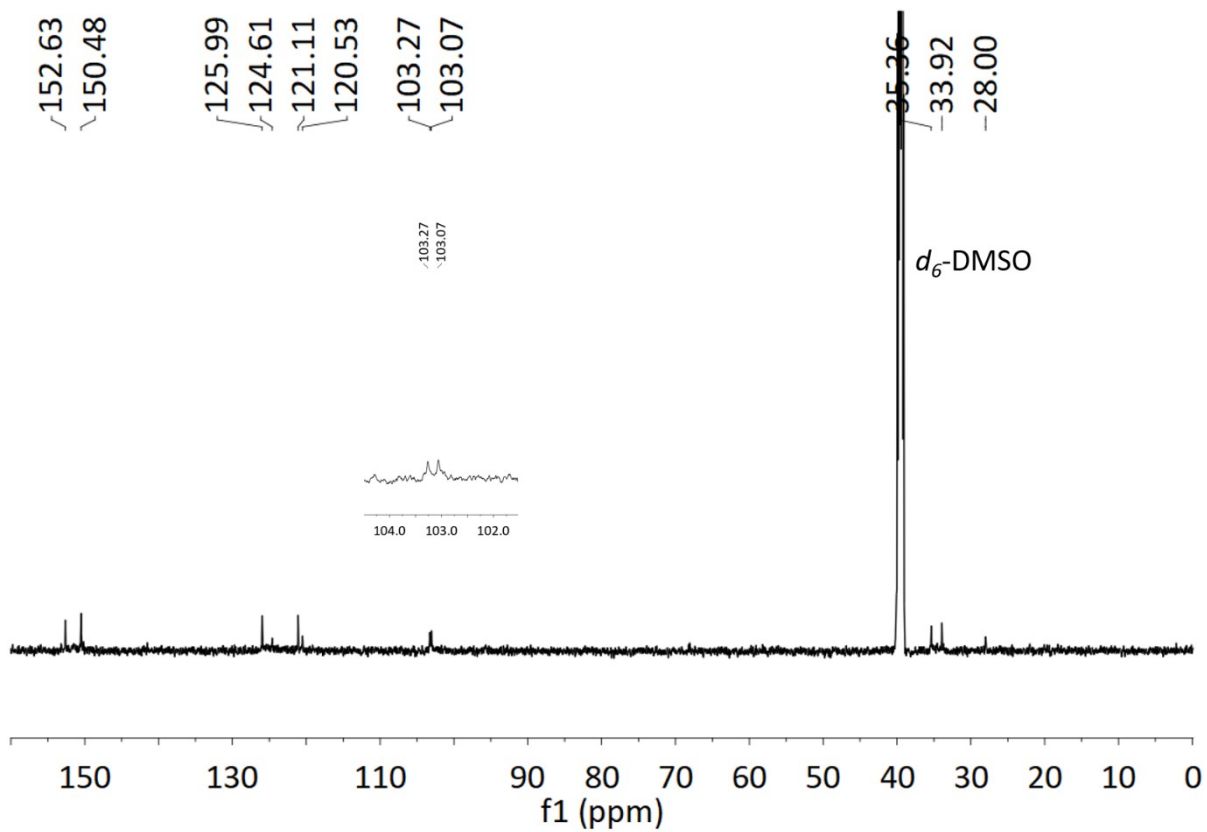
Figure S17. ^{13}C NMR spectrum of **Product 5.**

^{13}C NMR (600 MHz, d_6-DMSO): δC(ppm) 28.0, 33.9, 35.4, 103.1, 103.3, 120.5, 121.1, 124.6, 126.0, 150.5, 152.6
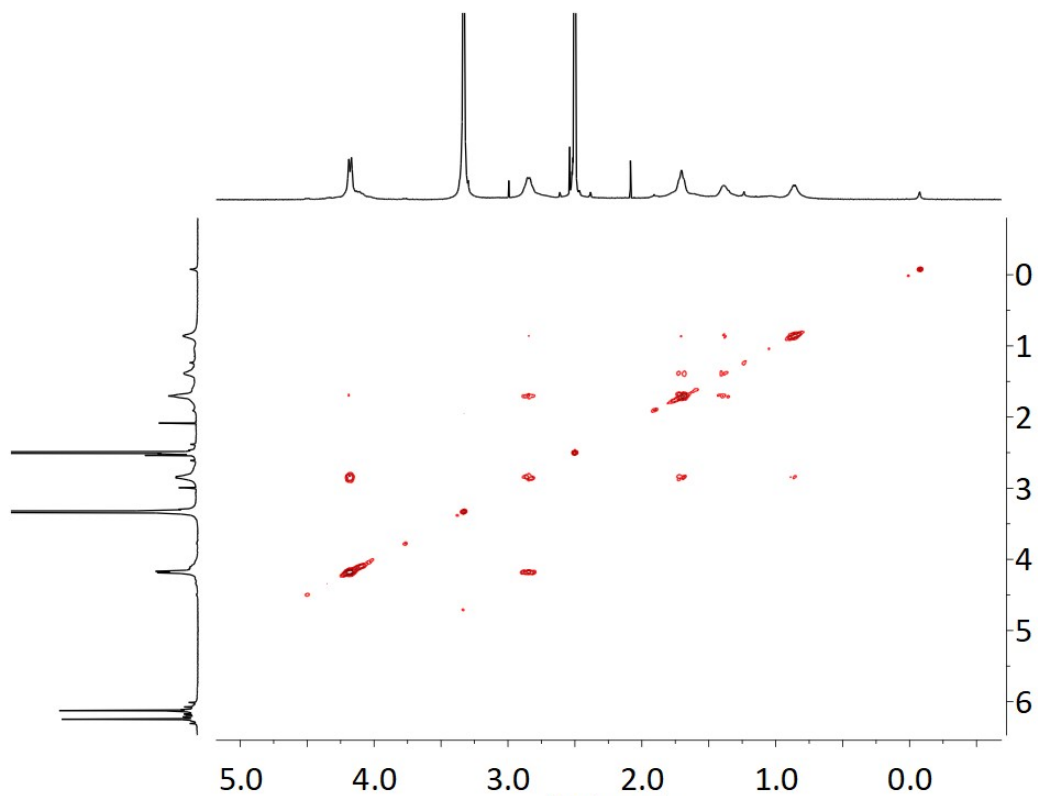
Figure S18. COSY NMR spectrum of **Product 5.**
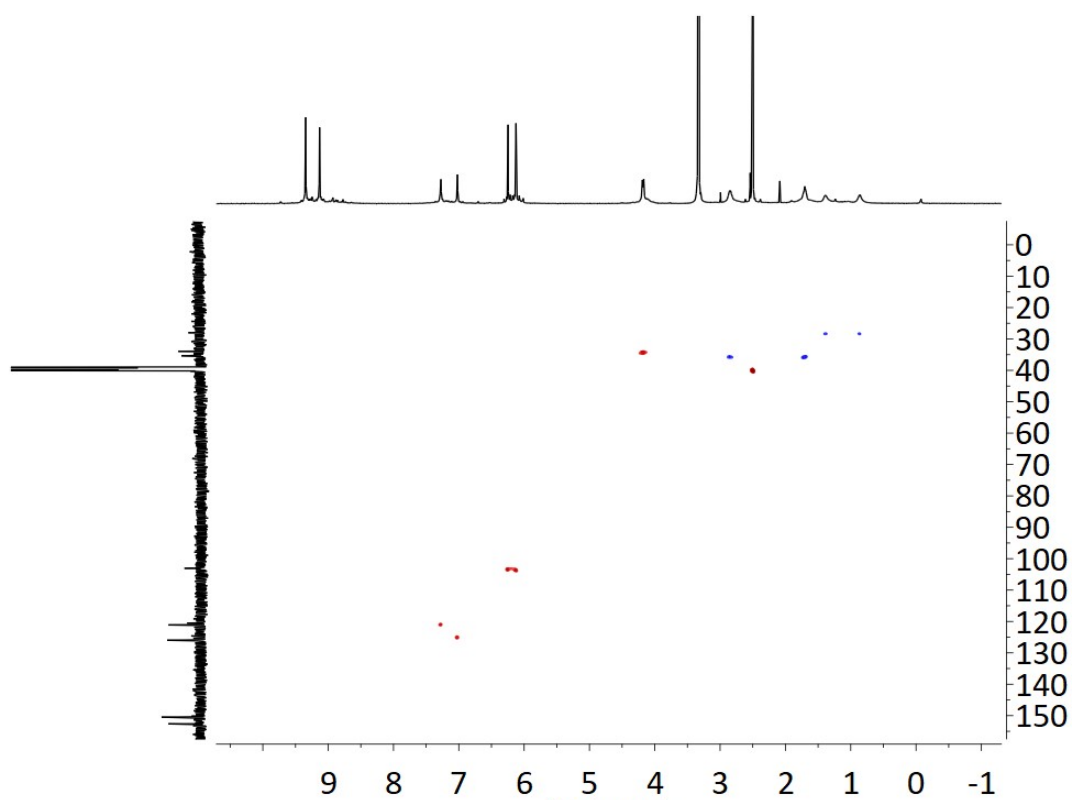
Figure S19. HSQC NMR spectrum of **Product 5.**
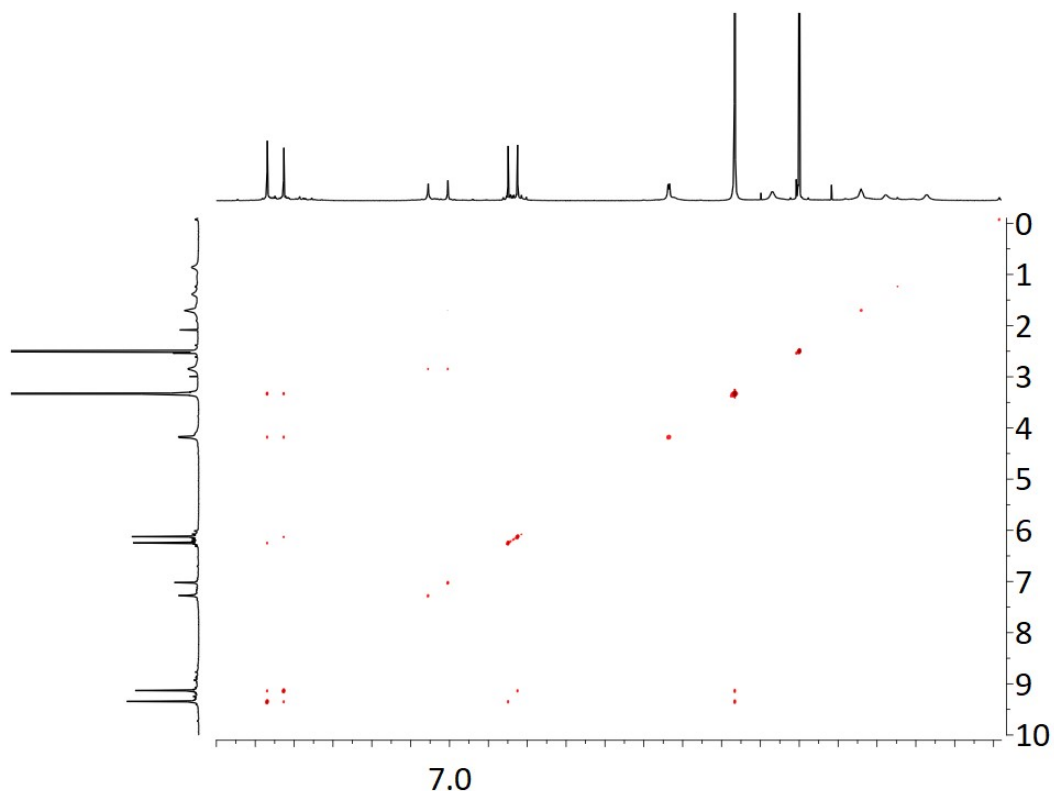
Figure S20. HMBC NMR spectrum of **Product 5.**
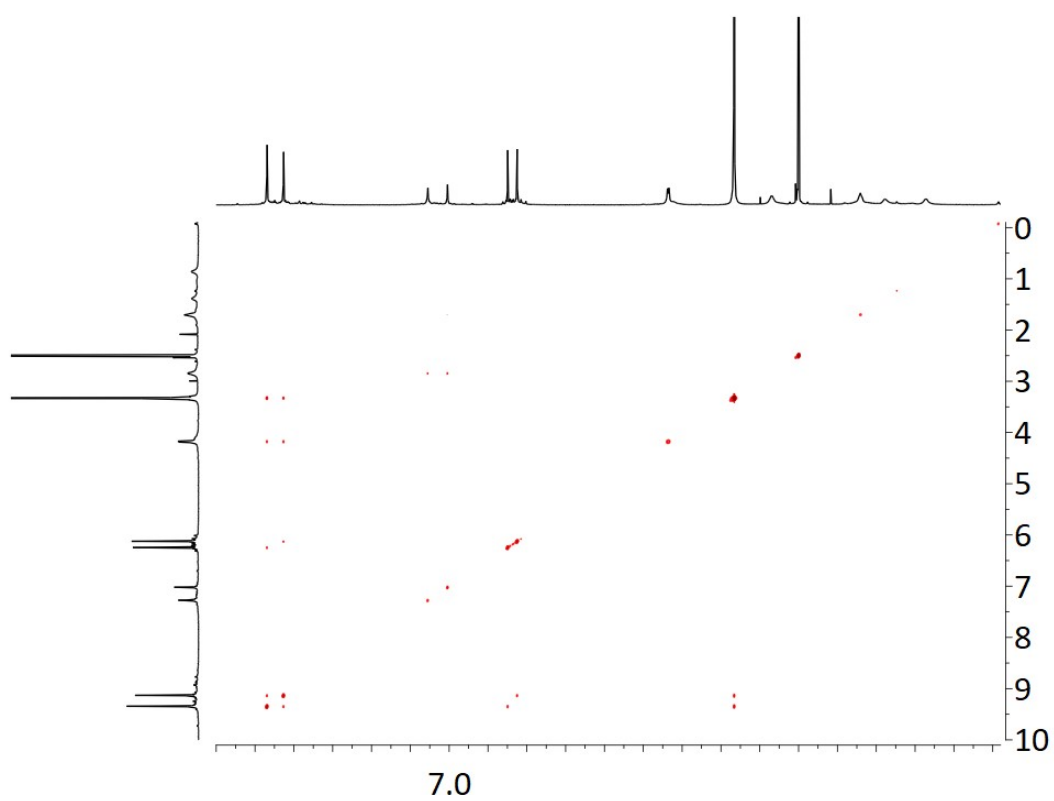
Figure S21. NOSEY NMR spectrum of **Product 5.**

S2.5.1 TGA for Product 5

Decomposition temperature = 342°C.
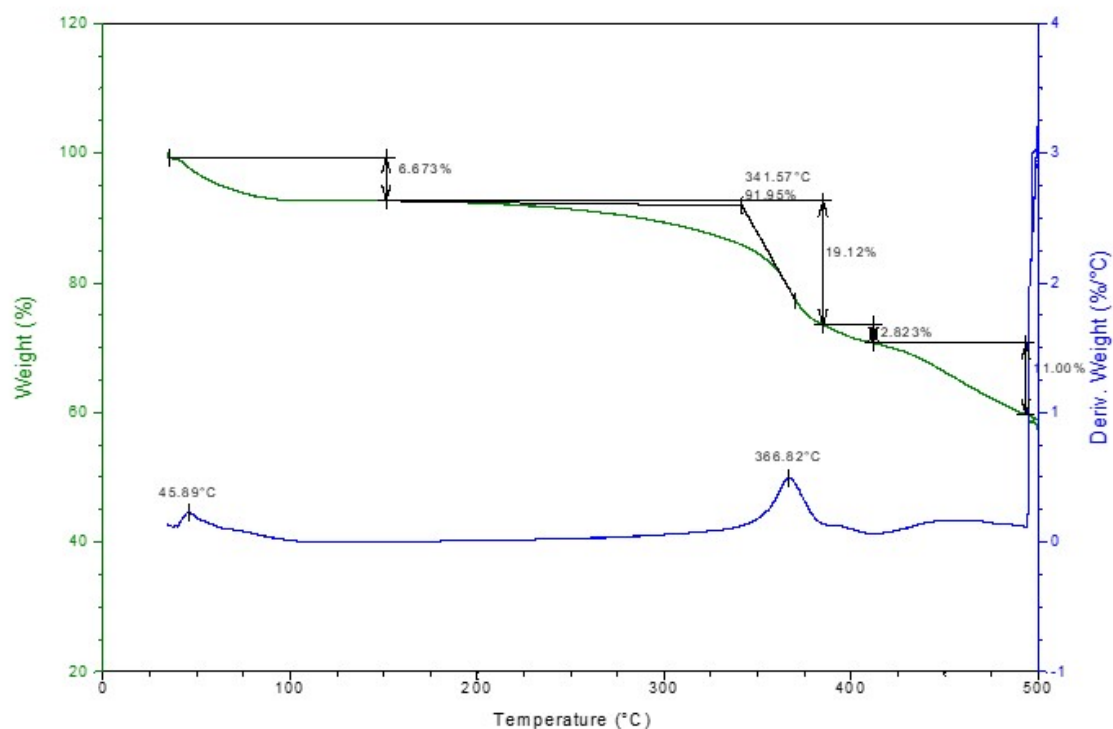
Figure S22. TGA for **Product 5**.

S2.6 Product 6

Soxhlet extraction was performed using 8 g of **Product 1** (crude Noria). **Product 6** was extracted under reflux at 80°C with 400 mL of MeOH for 9 days. After cooling to rt the MeOH solution was centrifuged (20 min, 4000 RPM). The solvent was decanted and concentrated *via* rotary evaporation to afford **Product 6** as an amber solid, which was dried under vacuum at 80°C overnight. (Crude yield 0.71 g, 8.9%)

Figure S23. ^{1}H NMR spectrum of **Product 6.**

S2.7 Single crystal growth of Product 7
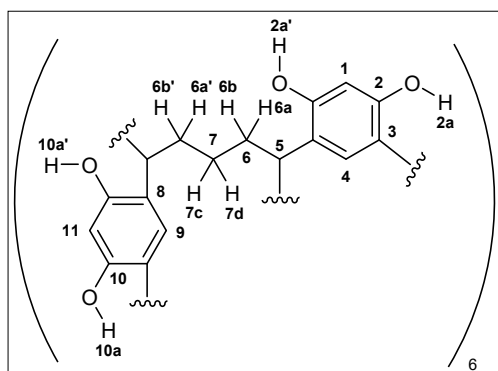
Product 6 was dissolved in a minimum of MeOH and added to a 1 mL vial which was capped with a punctured lid. This was placed in a 5 mL capped vial with Et$_2$O as the anti-solvent to allow vapour diffusion over the course of a few weeks. Single orange prism crystals of Noria (**Product 7**) were obtained. Refer to section S6.

Again, it should be noted that the structural diagram here is simplified and does not show the stereochemistry of Noria; H5 and H6a/a' are mutually *anti*, as are (H6a/a' and H7c) and (H6b/b' and H7d). The rim and side resorcinol units cannot be distinguished and therefore they have not been specified in the following assignment.
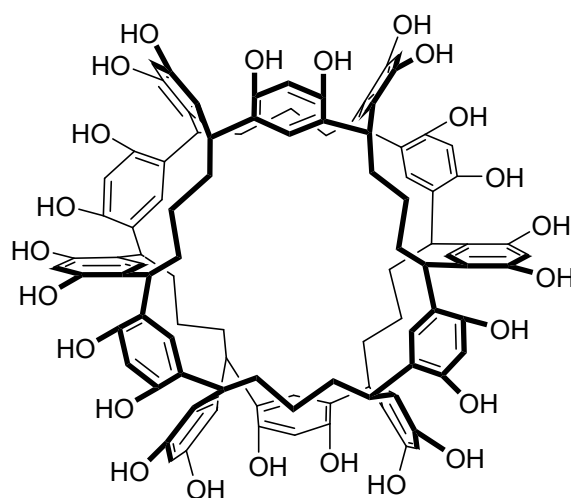
Figure S24. Full structure of Noria.
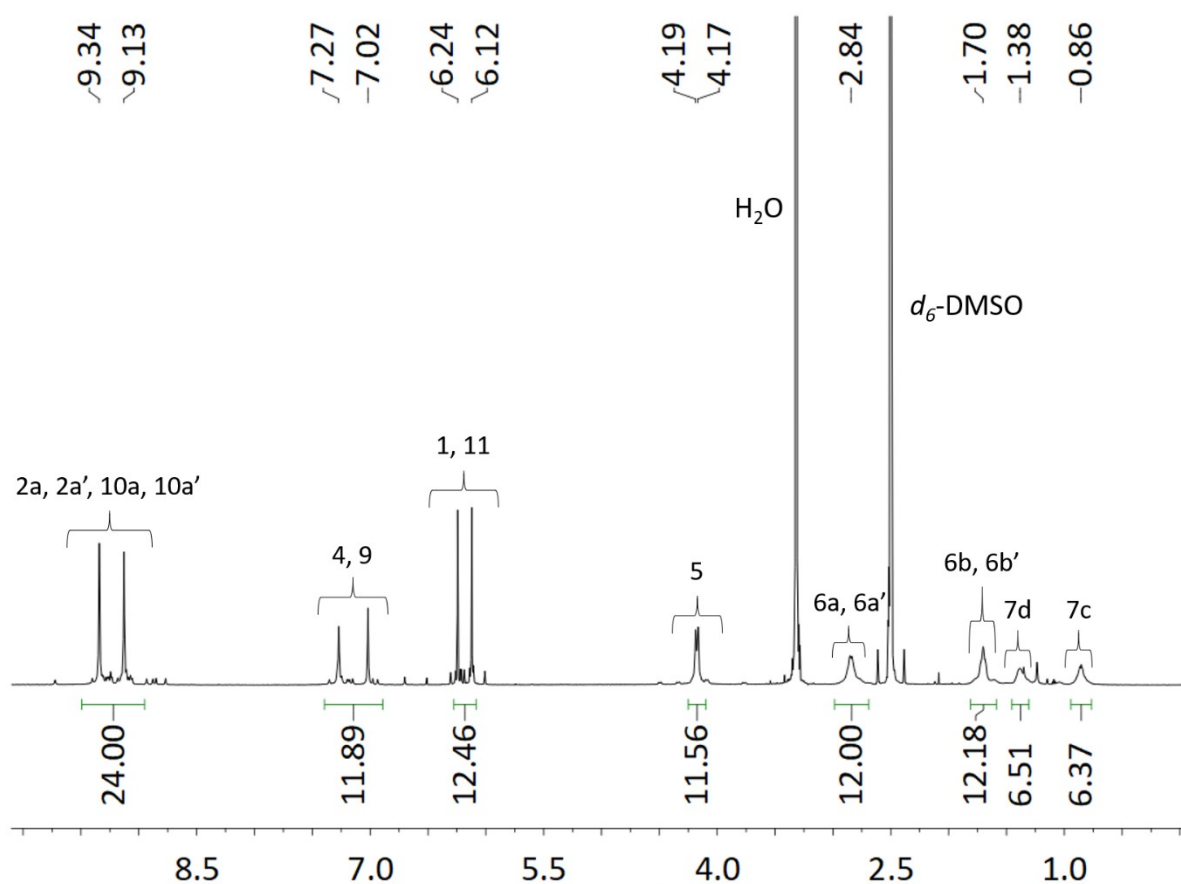
Figure S25. ¹H NMR spectrum of **Product 7.**

¹H NMR (600 MHz, d_6-DMSO): δH(ppm) 0.86 ppm (m, 6H, H_{7c}), 1.37 ppm (m, 6H, H_{7d}), 1.70 ppm (m, 12H, -CH_2-, H_{6b}, $H_{6b'}$), 2.84 ppm (m, 12H, -CH_2-, H_{6a}, $H_{6a'}$), 4.18 ppm (m, 12H, >CH-, H_5), 6.12-6.24 ppm (two s, 12H, Ar-H, H_1, H_{11}), 7.01-7.27 ppm (two s, 12H, Ar-H, H_4, H_9), 9.13-9.34 ppm (two s 24H, -OH, H_{2a}, $H_{2a'}$, H_{10a}, $H_{10a'}$)

S2.7.1 Mass spectrum for Product 7

nESI:

$[M + 2NH_4]^{2+}$, Theoretical: 870.3484 m/z, Observed: 870.3498 m/z
$[M + NH_4]^+$, Theoretical: 1722.6630 m/z, Observed: 1722.6640 m/z
$[M + Na]^+$, Theoretical: 1727.6184 m/z, Observed: 1727.6218 m/z

The lower portion of the spectrum is dominated by siloxane species that seem to be in the solvent blank, but weak doubly charged ammoniated and singly charged ammoniated and sodiated species were observed (**Figure S26** and **Figure S27**).
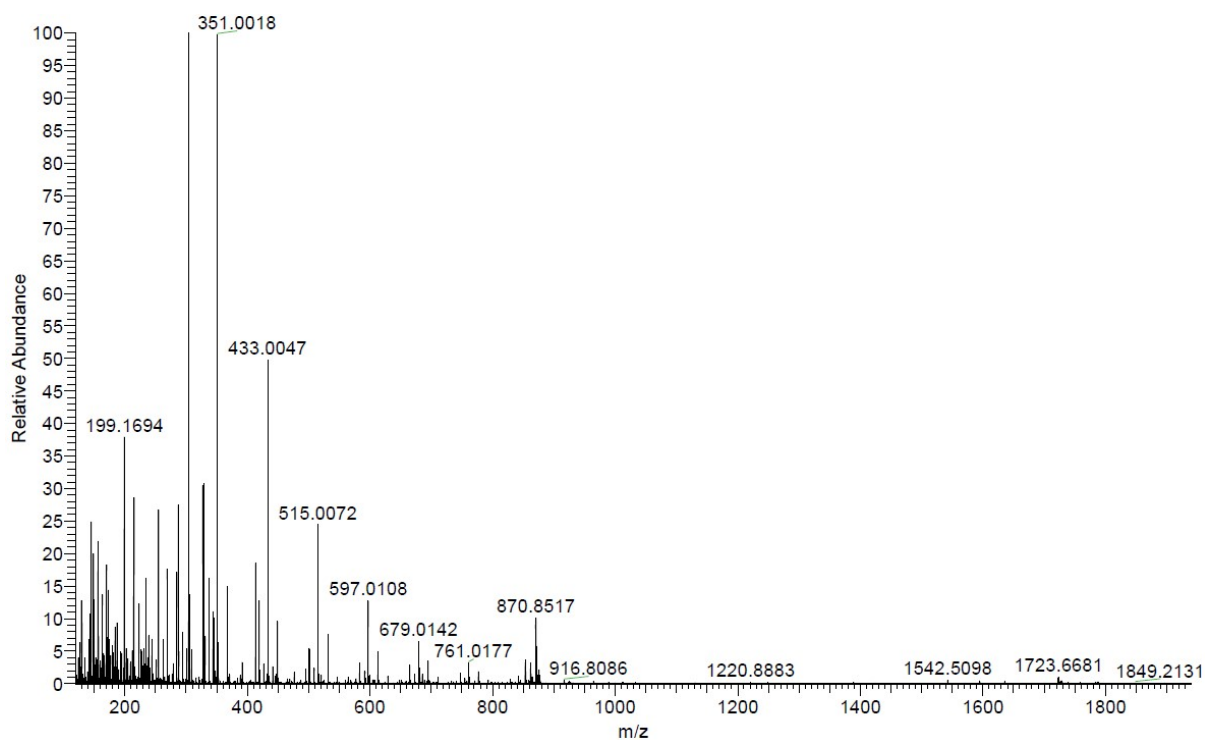
Figure S26. Mass spectrum of **Product 7** (nanoESI Positive (Orbitrap)).
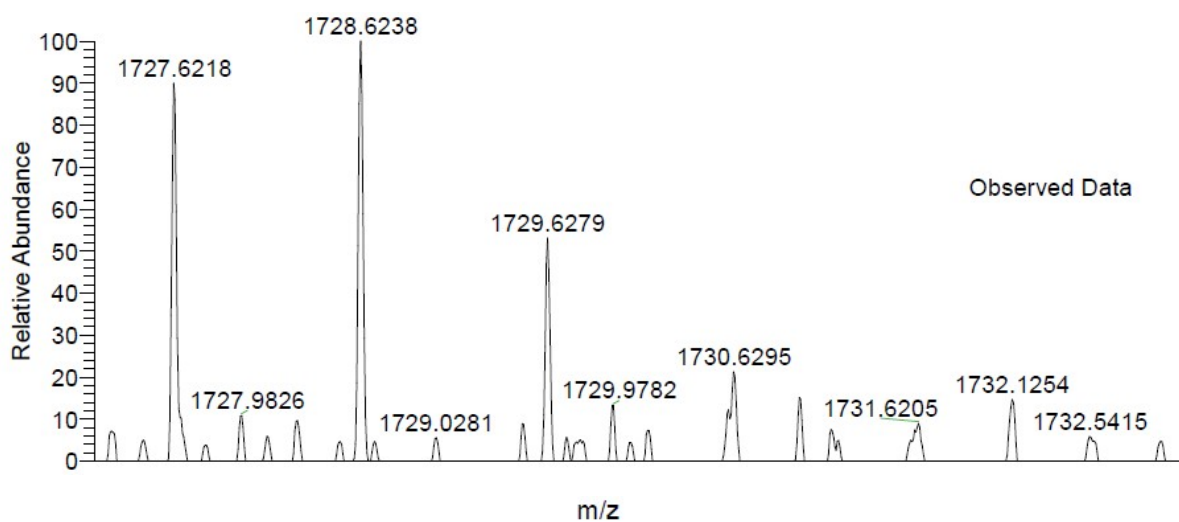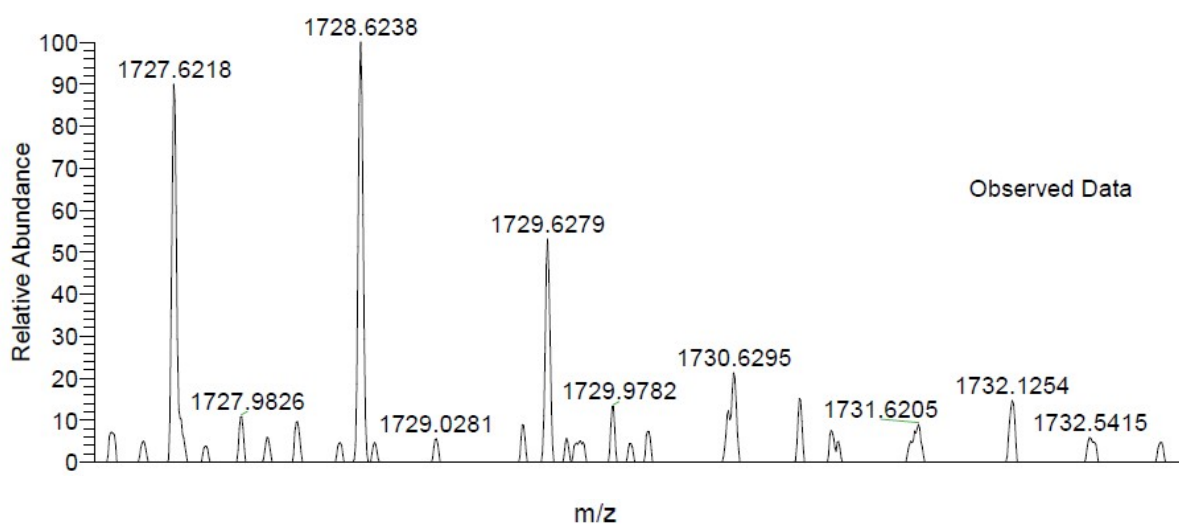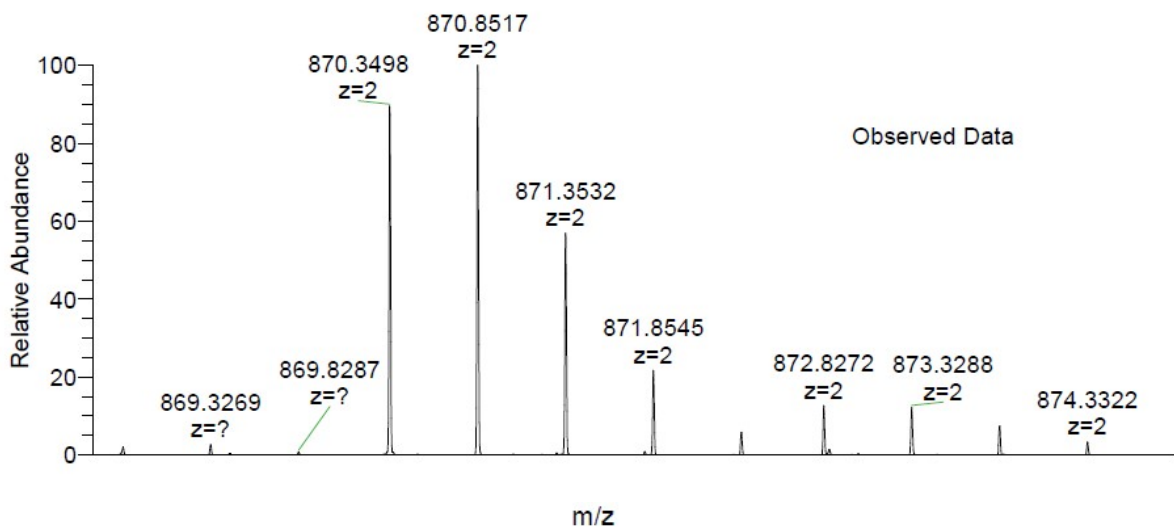
Figure S27. Zoomed Mass spectra of **Product 7** (nanoESI Positive (Orbitrap)).

S2.8 Overlay of ¹H NMR Spectra for Soxhlet Products
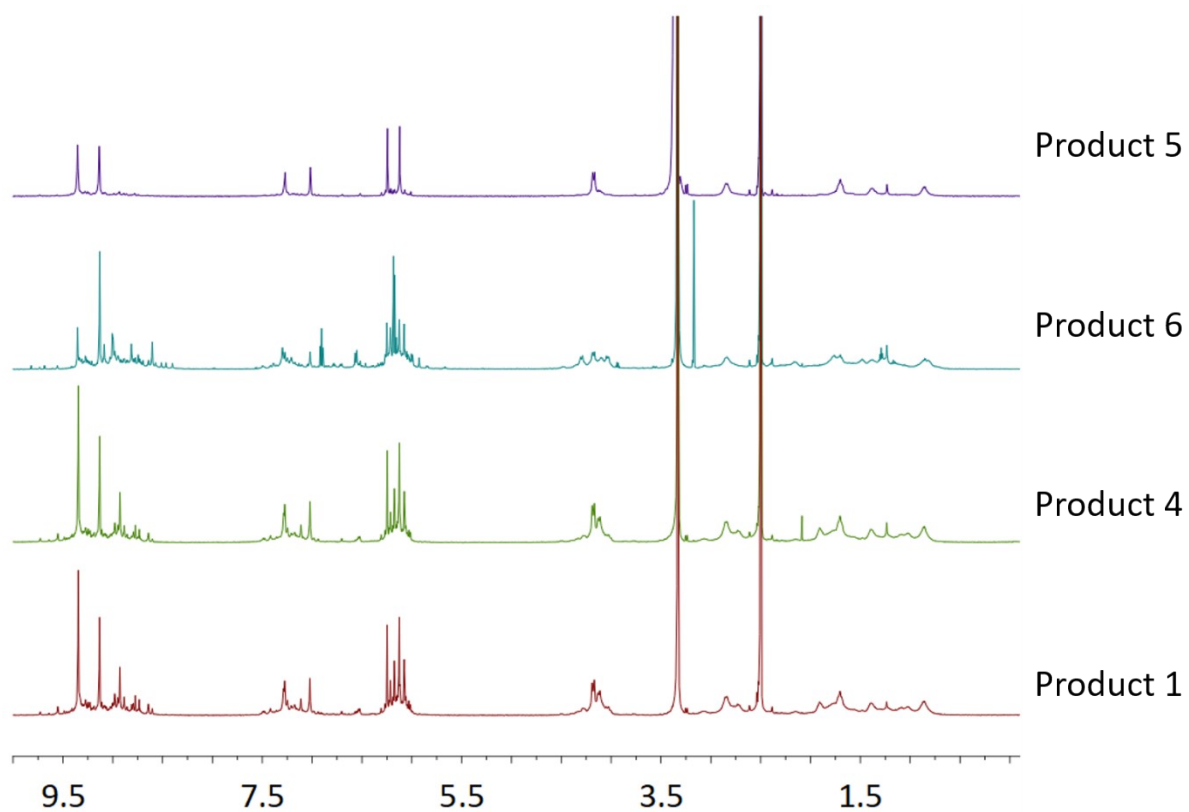
Figure S28. Overlay of ¹H NMR spectra of the Soxhlet Products (600 MHz).

S2.9 Overlay of ¹H NMR Spectra for Product 1, 2 and 7
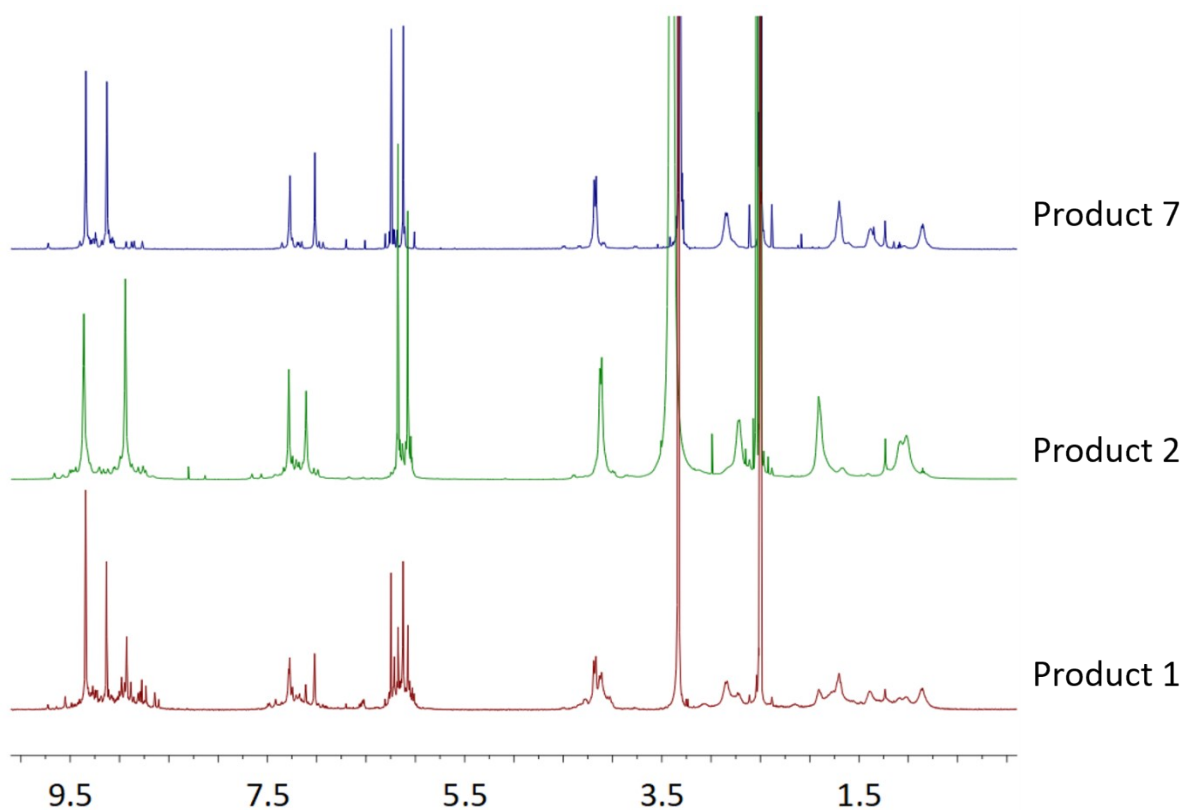
Figure S29. Overlay of Crude Noria (**Product 1**), Recrystallised Noria/Suspected Resorcinarene Trimer (R3) (**Product 2**) and Single Crystal of Noria (**Product 7**), showing that both Noria and R3 are present in the crude product (600 MHz).

S2.10 Variable Temperature ^{1}H NMR spectra (600 MHz) of Product 1
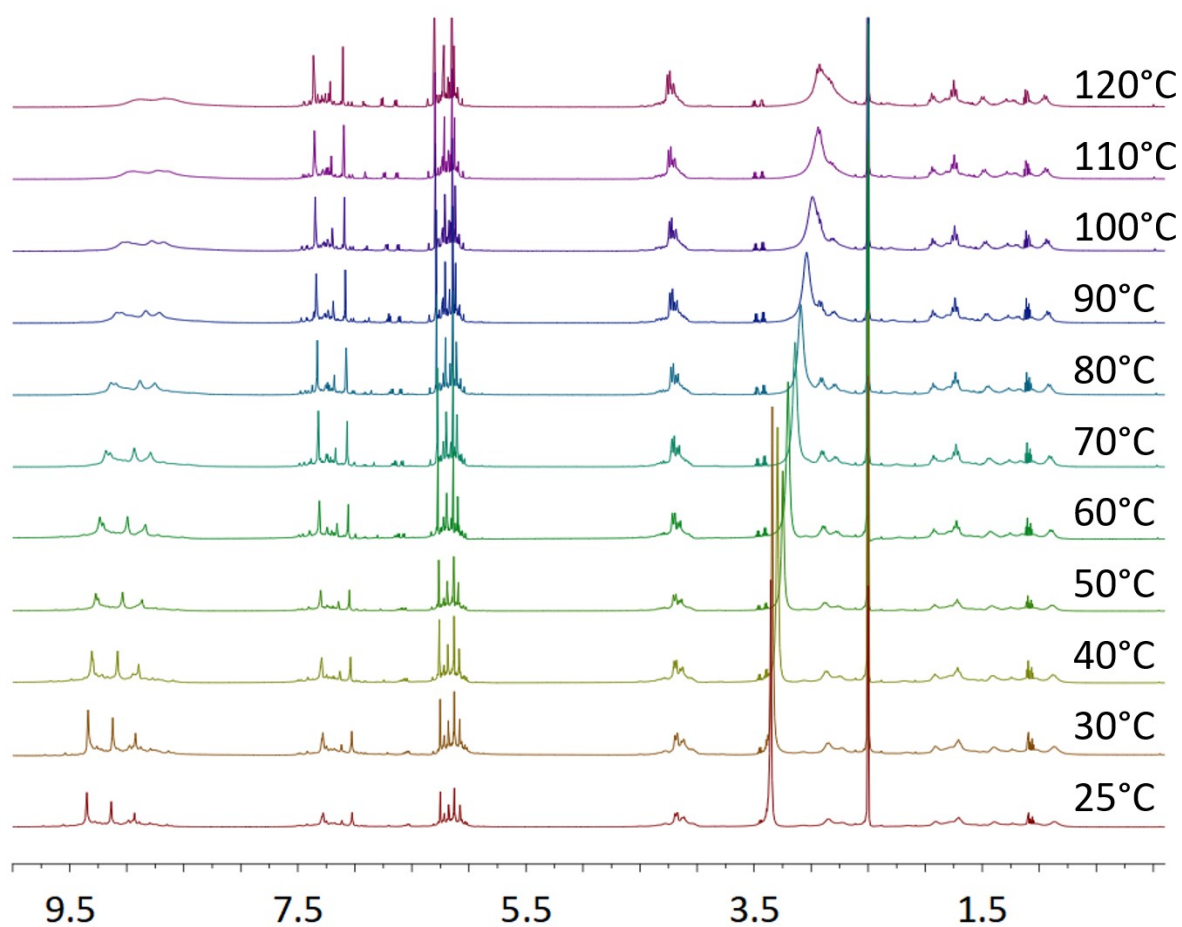
Figure S30. Overlay of Variable Temperature ^{1}H NMR spectra for **Product 1** (600 MHz).

S2.11 Product 5 Stability in Alkaline Conditions

Product 5 dissolved fully in D$_2$O in the presence of 25 equivalents of sodium hydroxide (NaOH). **Product 5**, which is mainly Noria, remains stable in aqueous alkaline solutions of > pH 10.
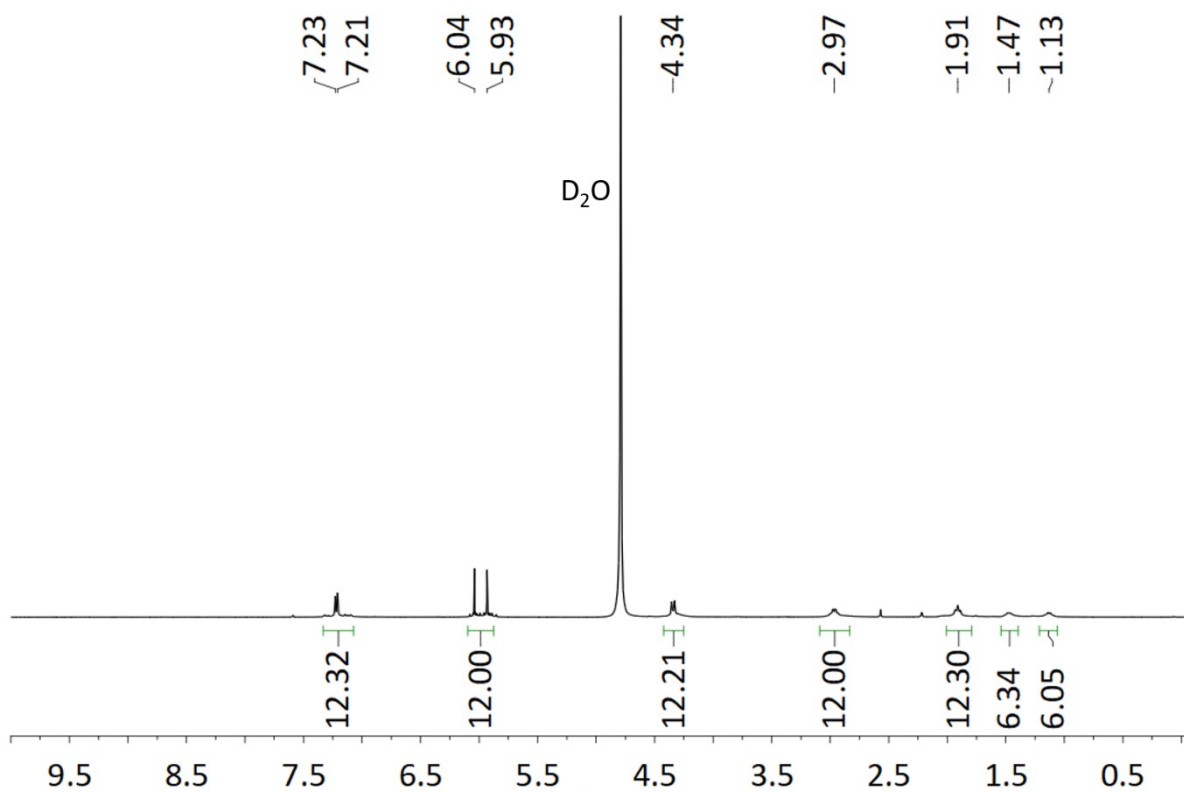
Figure S31. ^{1}H NMR spectrum of **Product 5** in aqueous alkaline solution.

S2.12 Overlay of ¹H NMR spectra for Noria heated over 7 days
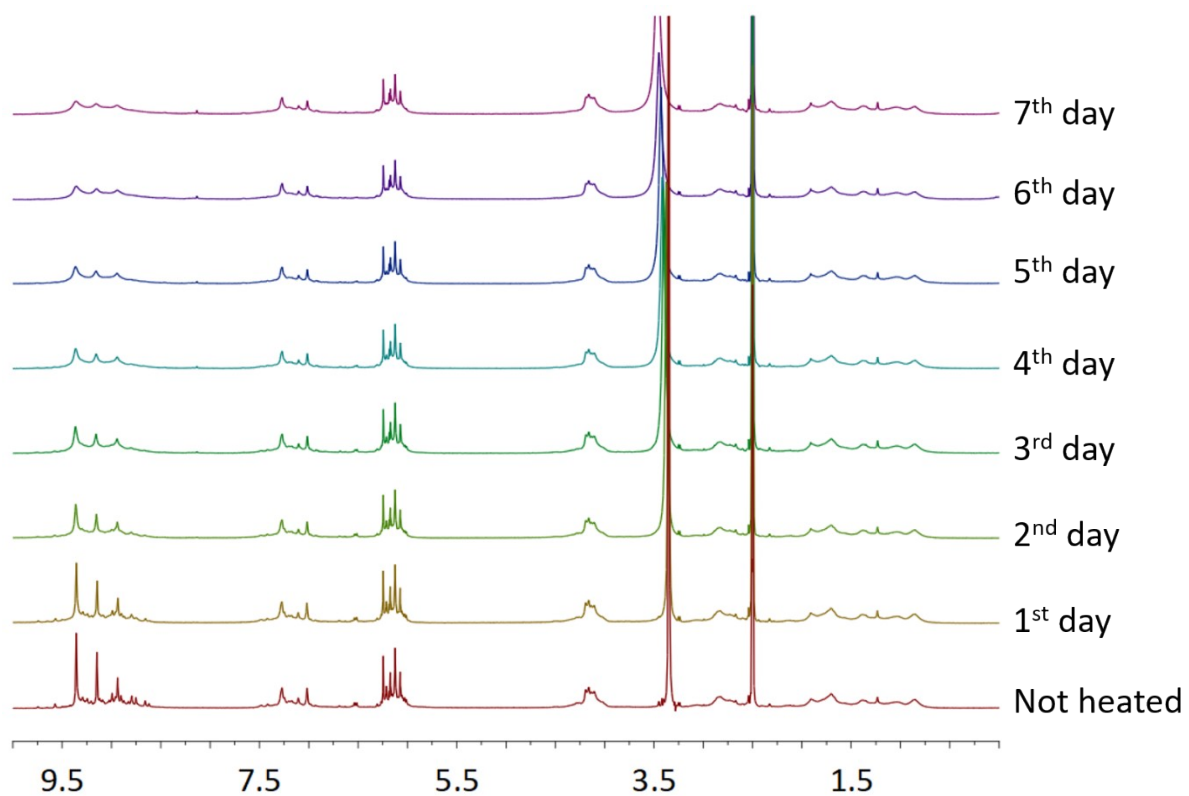
Figure S32. Overlay of ¹H NMR spectra of **Product 1** heated over several days at 100°C in wet d_6-DMSO.

S2.13 Synthesis of Noria-OEt
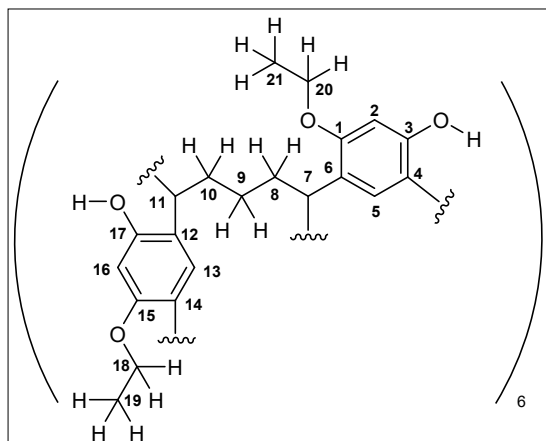
Noria-OEt was synthesised using a previously reported literature procedure.[2] To a RBF, 3-ethoxyphenol (11.0 g, 79.6 mmol), TFA (10 mL, 130.7 mmol) and $CHCl_3$ were added and agitated for 10 mins. Glutyraldehyde (1,5-Pentanedial, 50% in H_2O) (3.66 mL, 20.2 mmol) was then added slowly and the reaction mixture was refluxed at 80°C for 48 h. The reaction mixture was cooled to rt and poured into MeOH (150 mL). The suspension was filtered through a 4-pore sinter funnel with nylon filter paper and washed several times with Et_2O to afford Noria-OEt as a pale cream solid. The precipitated product was then dried in vacuum at 80°C overnight (Yield 4.39 g, 65%).
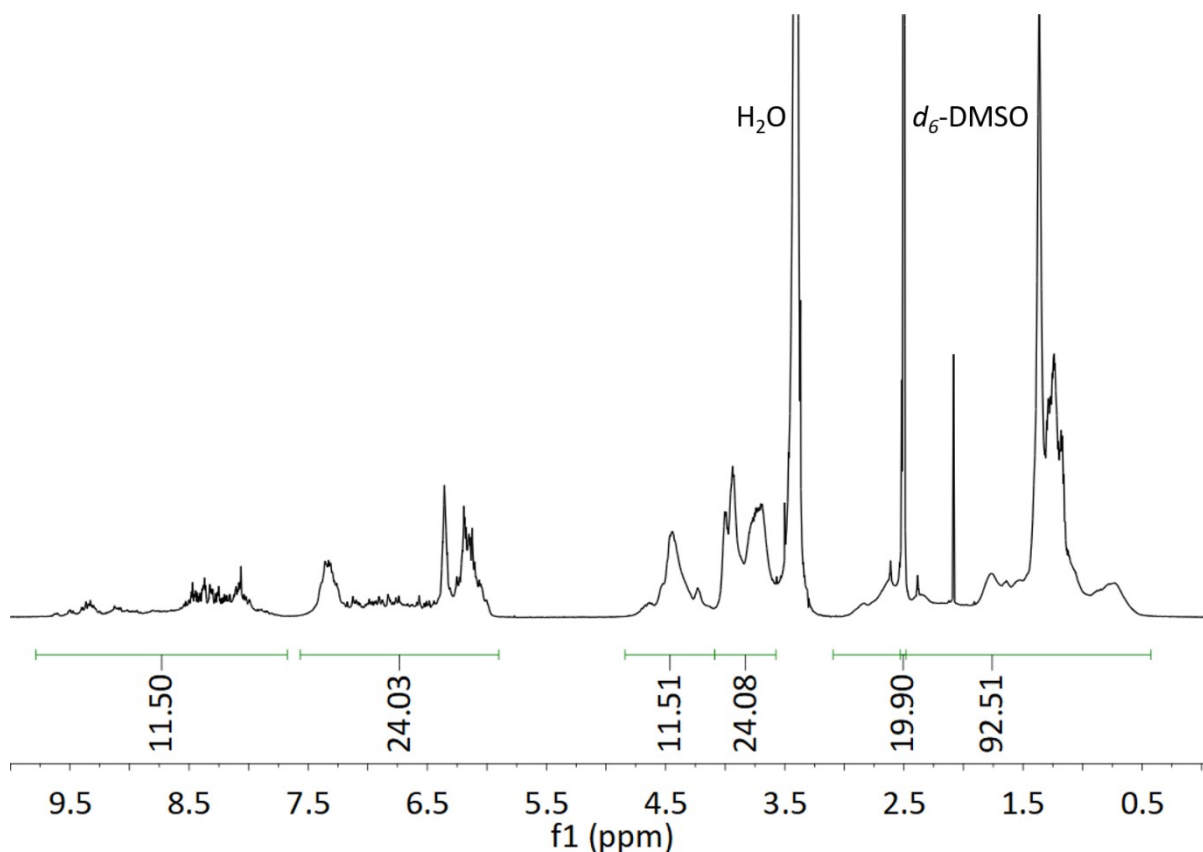
Figure S33. ^{1}H NMR spectrum of Noria-OEt.

^{1}H NMR (600 MHz, d_6-DMSO): δH(ppm) 0.43-3.09 ppm (m, 72H (should be 72H), $-CH_2CH_2CH_2-$, H_8, H_9, H_{10}, $-CH_3$, H_{19}, H_{21}), 3.58-4.09 ppm (m, 24H, $-OCH_2-$, H_{18}, H_{20}), 4.09-4.84 ppm (m, 12H, >CH-, H_7, H_{11}), 5.89-7.57 ppm (m, 24H, Ar-H, H_2, H_5, H_{13}, H_{16}), 7.68-9.78 ppm (m, 12H, OH, H_3, H_{17}). The ^{1}H NMR spectrum was shown to be consistent with that reported.[2]

S2.13.1 Mass spectrum for Noria-OEt

MALDI-TOF:

The expected radical molecular species was observed, as well as sodiated and potassiated analogues.

[M]$^{+\bullet}$, Theoretical: 2041.0 m/z, Observed: 2040.7 m/z
[M + Na]$^{+}$, Theoretical: 2064.0 m/z, Observed: 2064.7 m/z
[M + K]$^{+}$, Theoretical: 2080.0 m/z, Observed: 2080.7 m/z

Again, the increase of 250 mass units may relate to a potential complex with DCTB from the DCTB

Matrix that was used (**Figure S12**). It is possible that DCTB may reside inside the cavity of Noria-OEt.
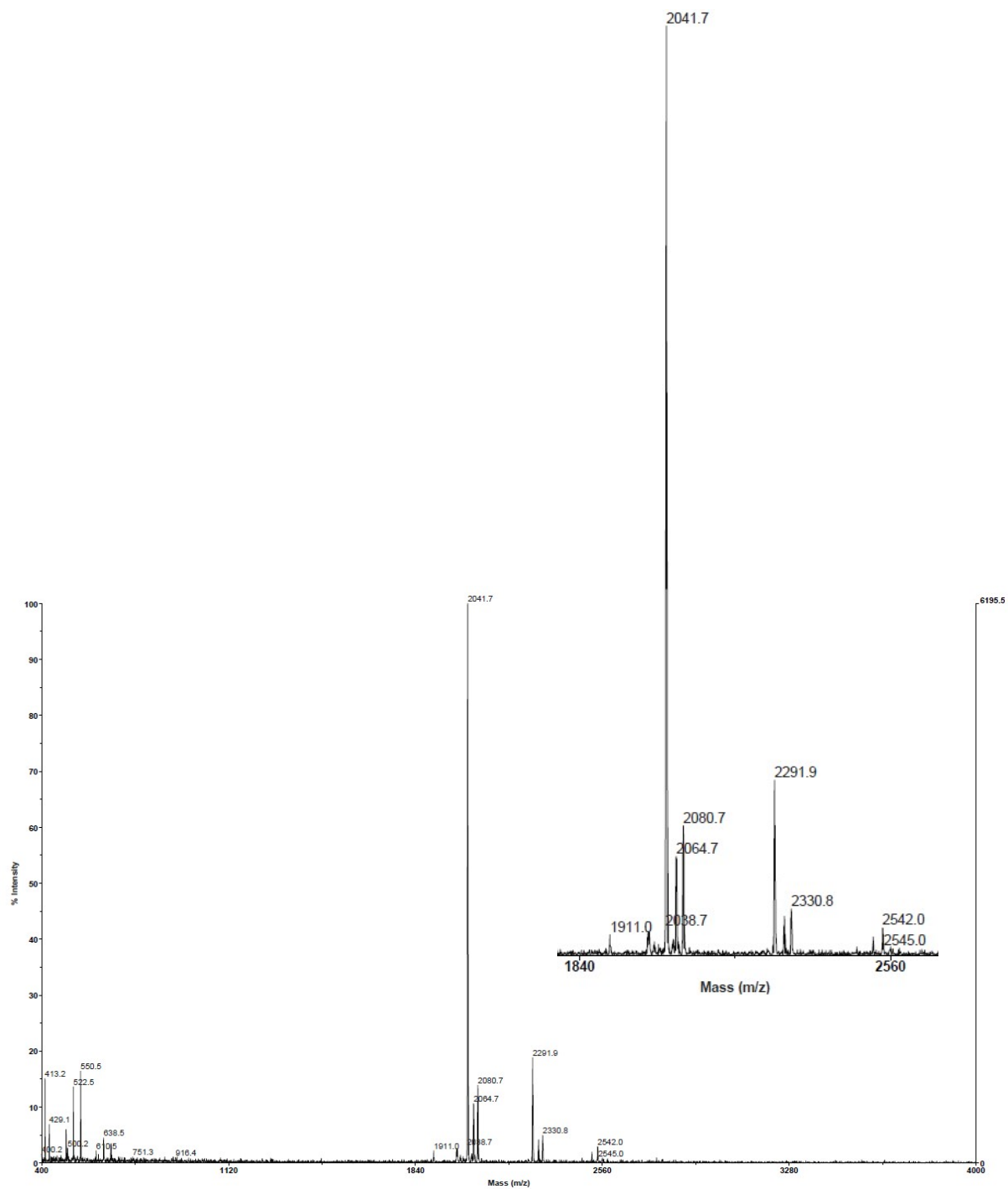
Figure S34. Noria-OEt mass spectrum (solvent-free-MALDI (Voyager)).

S2.13.2 TGA for Noria-OEt

TGA: decomposition temperature = 340°C.
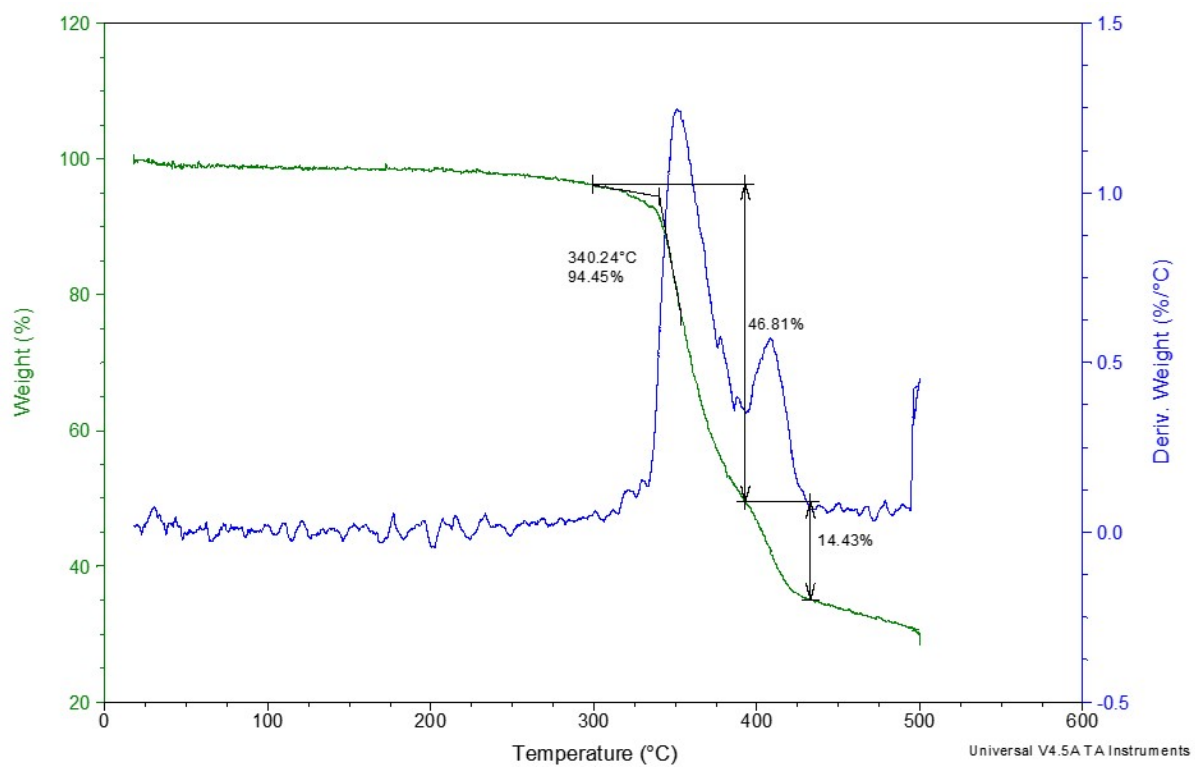
Figure S35. TGA of Noria-OEt.

S2.13.3 Geometrical Isomers of Noria-OEt

Side Resorcinol residues
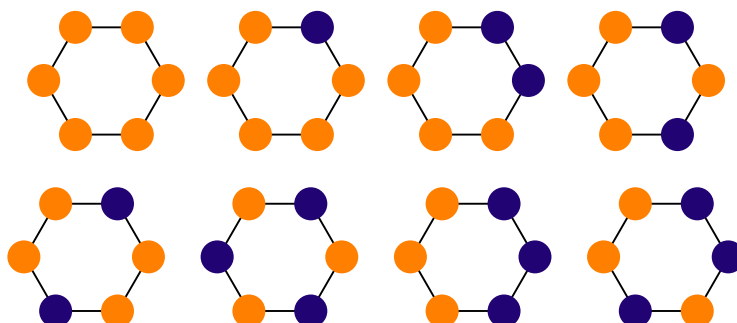
● = Ethoxy group pointing up

● = Ethoxy group pointing down

Rim Resorcinol residues
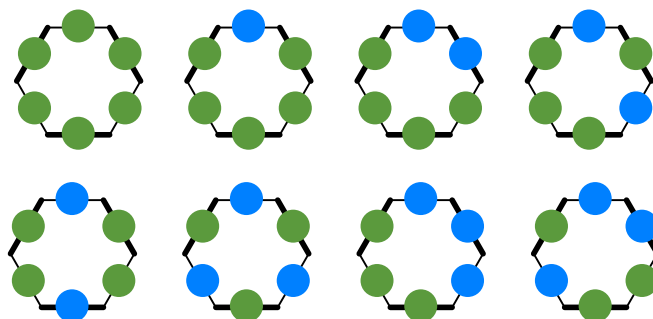
● = Ethoxy group pointing clockwise

● = Ethoxy group pointing anti-clockwise

╱ = Upper Rim

╱ = Lower Rim

Figure S36. Isomers of Noria-OEt.

There are 8 potential 'side' isomers and 8 potential 'rim' isomers and therefore there are 64 potential geometrical isomers.

S2.14 ¹H NMR spectrum of Noria as reported by Shimoyama et al.
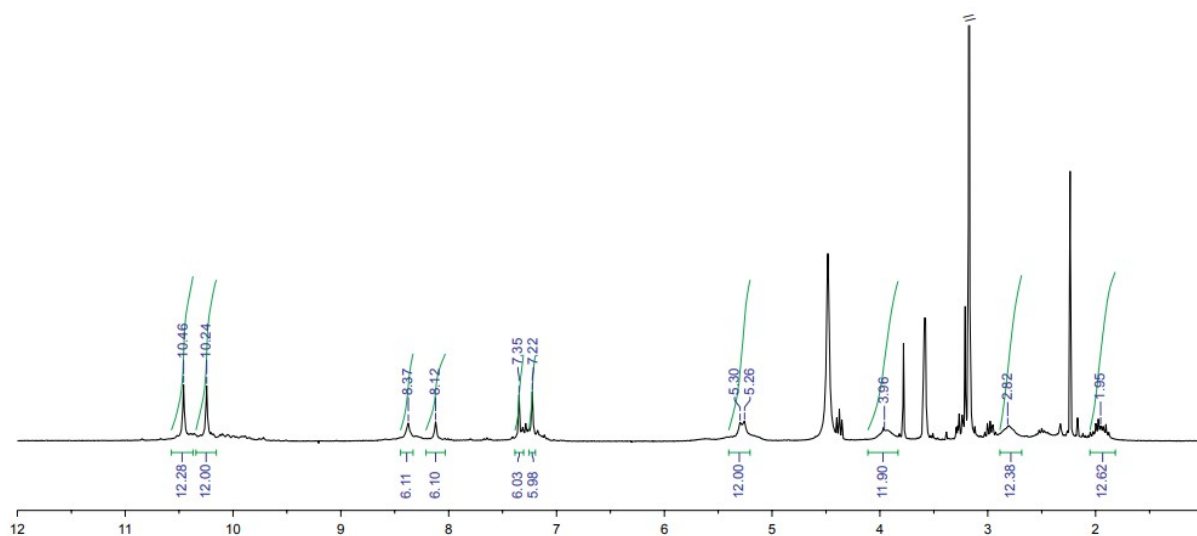
Figure S37. ¹H NMR spectrum of Noria reported by Shimoyama et al. Reproduced from reference 3.

S3. Synthesis of Noria-OEt Porous Liquid

To form the Noria-OEt PL, activated porous Noria-OEt (50 mg) was dissolved in dry 15-crown-5 (1 ml) by sonication until a clear amber solution had formed (**Figure S38**).

Figure S38. Formation of **Noria-OEt PL**.

S3.1 Viscosity of Noria-OEt PL

25.7 mPa·s at 20.4°C

S3.2 Density of Noria-OEt PL

1.12 g/mL at 20°C

S3.3 Brunauer–Emmett–Teller (BET) analysis

The calculated BET surface area from N_2 sorption at 77 K is 105.118 $m^2 g^{-1}$.
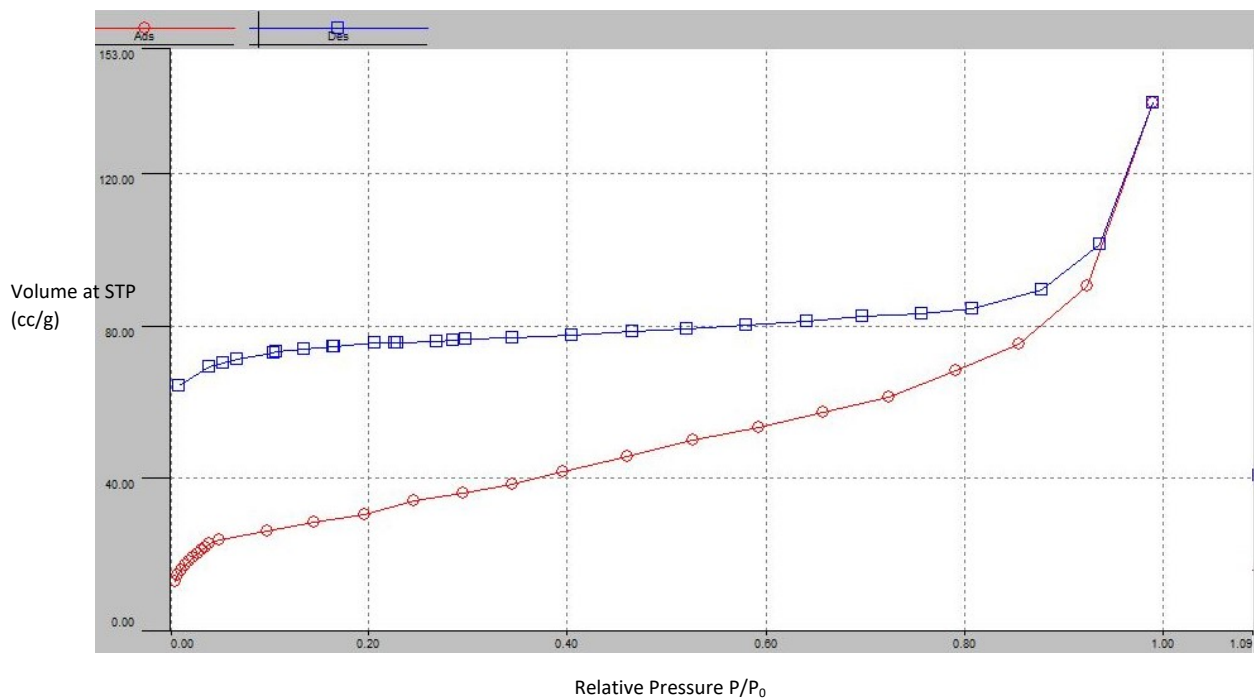
Figure S39. Type IV Isotherm of Noria-OEt.

S4. Barometric Gas Solubility Measurements

S4.1 Noria-OEt PL

The solubility measurements of methane (CH_4) in both 15-crown-5 and the PL at 303.15 K and 1-5 bar were measured on the barometric gas rig apparatus (**Figure S40**).[4]
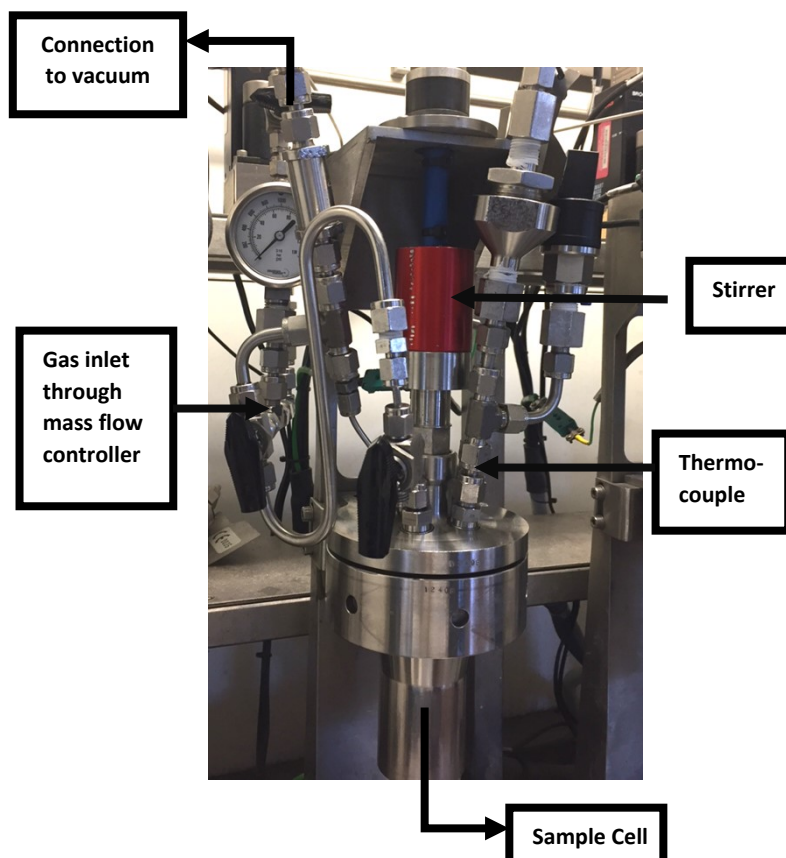
Figure S40. Barometric gas rig apparatus.

20 mL of the samples were added into the sample cell and the samples were degassed for two hours. The samples were stirred at 1400 rpm at 303.15 K and measurements were left to stabilise at each pressure point for 1 hour. The process makes use of a constant temperature and pressure while directly measuring the volume of gas needed to maintain the pre-set conditions. The volume of gas needed directly corresponds to the amount gas adsorbed by the materials (See Tables below).

Table S1. CH_4 Uptake of 15-crown-5 at 303.15 K (values given to 4 d.p.).

Pressure (bar)	CH₄ Uptake of 15-crown-5 1ˢᵗ Run (mg/g)	CH₄ Uptake of 15-crown-5 2ⁿᵈ Run (mg/g)	CH₄ Uptake of 15-crown-5 3ʳᵈ Run (mg/g)	Average CH₄ Uptake of 15-crown-5 (mg/g)	Standard Deviation
1 bar	0.1322	0.1125	0.1338	0.1262	0.0097
2 bar	0.2625	0.2360	0.2527	0.2504	0.0110
3 bar	0.4177	0.3730	0.4640	0.4183	0.0372
4 bar	0.5944	0.5434	0.7126	0.6168	0.0709
5 bar	0.8520	0.8194	0.9836	0.8850	0.0710

Table S2. CH_4 Uptake of Noria-OEt PL at 303.15 K (values given to 4 d.p.).

Pressure (bar)	CH₄ Uptake of Noria-OEt PL 1ˢᵗ Run (mg/g)	CH₄ Uptake of Noria-OEt PL 2ⁿᵈ Run (mg/g)	CH₄ Uptake of Noria-OEt PL 3ʳᵈ Run (mg/g)	Average CH₄ Uptake of Noria-OEt PL (mg/g)	Standard Deviation
1 bar	0.2685	0.2276	0.1443	0.2135	0.0517
2 bar	0.4708	0.3755	0.3515	0.3993	0.0515
3 bar	0.7056	0.6568	0.5704	0.6443	0.0559
4 bar	0.8553	0.8551	0.8313	0.8472	0.0113
5 bar	1.1552	1.2721	1.1322	1.1865	0.0612

Table S3. Enhanced CH_4 Uptake of Noria-OEt PL at 303.15 K (values given to 4 d.p.).

Pressure (bar)	15-crown-5 Average CH₄ Uptake (mg/g)	Noria-OEt PL Average CH₄ Uptake (mg/g)	Enhanced CH₄ Uptake of Noria-OEt PL (mg/g) (Difference between Noria-OEt PL and 15-crown-5)
1 bar	0.1262	0.2135	0.0873
2 bar	0.2504	0.3993	0.1489
3 bar	0.4183	0.6443	0.2260
4 bar	0.6168	0.8472	0.2304
5 bar	0.8850	1.1865	0.3015

Table S4. Average Number of CH_4 Molecules per Noria-OEt cavity.

Pressure (bar)	Difference in uptake between 15-crown-5 and Noria-OEt PL (mg/g) (4 d.p.)	Average moles of CH_4 actually adsorbed by Noria-OEt	Average Number of CH_4 Molecules per Noria-OEt cavity (2 d.p.)
1 bar	0.0873	5.442×10^{-6}	0.22
2 bar	0.1489	9.281×10^{-6}	0.38
3 bar	0.2260	1.409×10^{-5}	0.58
4 bar	0.2304	1.437×10^{-5}	0.59
5 bar	0.3015	1.880×10^{-5}	0.77

Moles of Noria-OEt present in the PL = 2.448×10^{-5} moles

S4.2 Control Experiment – Monomer

A control experiment was conducted using the monomer 3-ethoxyphenol to ensure that the enhanced CH_4 solubility seen for the PL cannot be ascribed to a simple solvating effect of the aromatic cage walls of Noria-OEt.

The monomer solution was prepared by adding 3-ethoxyphenol (40.6 mg) to dry 15-crown-5 (1 ml) and sonicating until fully dissolved.

The solubility measurements of CH_4 in both 15-crown-5 and the monomer at 303.15 K and 1-5 bar were measured on the barometric gas rig apparatus (**Figure S40**) using the same method as was described in section S4.1.

Table S5. CH_4 Uptake of 15-crown-5, used to make monomer solution, at 303.15 K (values given to 4 d.p.) (Same as Table S1).

Pressure (bar)	CH_4 Uptake of 15-crown-5 1st Run [mg/g]	CH_4 Uptake of 15-crown-5 2nd Run (mg/g)	CH_4 Uptake of 15-crown-5 3rd Run (mg/g)	Average CH_4 Uptake of 15-crown-5 (mg/g)	Standard Deviation
1 bar	0.1322	0.1125	0.1338	0.1262	0.0097
2 bar	0.2625	0.2360	0.2527	0.2504	0.0110
3 bar	0.4177	0.3730	0.4640	0.4183	0.0372
4 bar	0.5944	0.5434	0.7126	0.6168	0.0709
5 bar	0.8520	0.8194	0.9836	0.8850	0.0710

Table S6. CH_4 Uptake of Monomer solution at 303.15 K (values given to 4 d.p.).

Pressure (bar)	CH_4 Uptake of monomer 1st Run (mg/g)	CH_4 Uptake of monomer 2nd Run (mg/g)	CH_4 Uptake of monomer 3rd Run (mg/g)	Average CH_4 Uptake of monomer (mg/g)	Standard Deviation
1 bar	0.1049	0.0658	0.0974	0.0894	0.0170
2 bar	0.2589	0.2374	0.2389	0.2451	0.0098
3 bar	0.4396	0.3839	0.4311	0.4182	0.0245
4 bar	0.6088	0.5886	0.6546	0.6173	0.0276
5 bar	0.9487	0.7887	0.9260	0.8878	0.0707

Table S7. 'Enhanced' CH_4 Uptake of Monomer at 303.15 K (values given to 4 d.p.).

Pressure (bar)	15-crown-5 Average	Monomer Average	'Enhanced' CH_4 Uptake of Monomer (mg/g) (Difference between Monomer and 15-crown-5)
1 bar	0.1262	0.0894	-0.0368
2 bar	0.2504	0.2451	-0.0053
3 bar	0.4183	0.4182	-0.0001
4 bar	0.6168	0.6173	0.0005
5 bar	0.8850	0.8878	0.0028
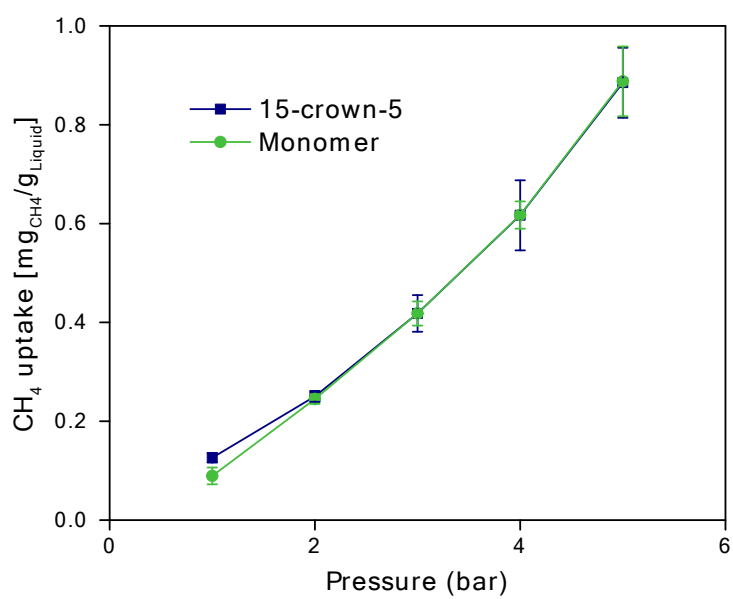
Figure S41. CH$_4$ uptake at 303.15 K for 15-crown-5 average compared to Monomer in 15-crown-5 (40.6 mg/mL) average (1-5 bar).

S5. Models and force-fields parameters
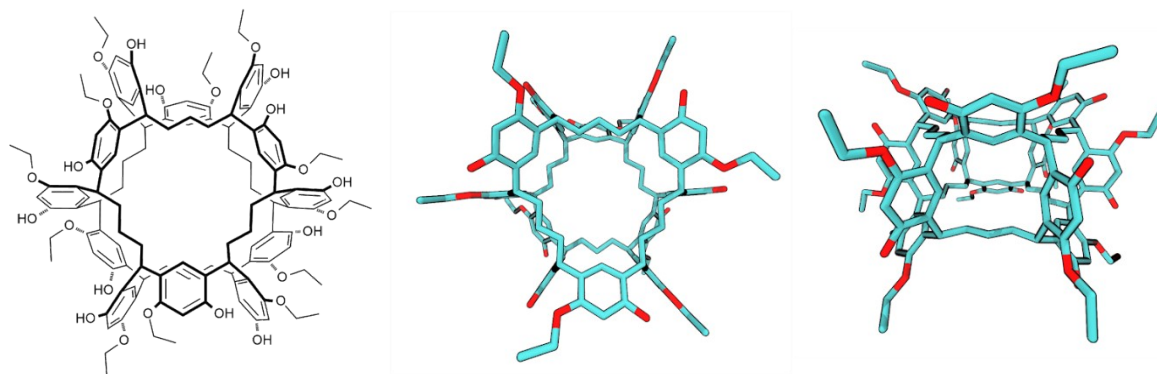
Figure S42. 2D and 3D representation of the Noria-OEt isomer employed to build the PL system for Molecular Dynamic simulations. In the 3D representation, hydrogen atoms are omitted for the sake of clarity.
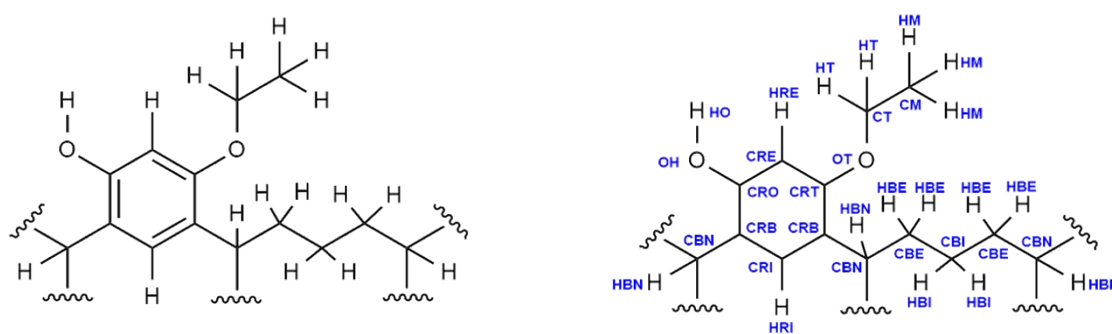
Figure S43. Representation of the recurring structure of the Noria-OEt host. The labels on the right correspond to force-field atom types, as defined in **Table S8**.

Table S8. Atom types, point charges and Lennard-Jones parameters for Noria-OEt.

Atom type	Mass	Charge (e)	Sigma (nm)	Epsilon (kj/mol)
HM	1.00800	0.059124	0.2500000	0.1255200
CM	12.01100	-0.182898	0.3500000	0.2761440
CT	12.01100	0.064514	0.3500000	0.2761440
HT	1.00800	0.060185	0.2500000	0.1255200
OT	15.99940	-0.148014	0.2900000	0.5857600
CRT	12.01100	-0.013342	0.3550000	0.2928800
CRE	12.01100	-0.123588	0.3550000	0.2928800
CRO	12.01100	0.070264	0.3550000	0.2928800
CRB	12.01100	-0.027644	0.3550000	0.2928800
CRI	12.01100	-0.221196	0.3550000	0.2928800
HRE	1.00800	0.127035	0.2420000	0.1255200
HRI	1.00800	0.142915	0.2420000	0.1255200
OH	15.99940	-0.449749	0.3070000	0.7112800
HO	1.00800	0.351587	0.0000000	0.000000
CBN	12.01100	0.142446	0.3500000	0.2761440
HBN	1.00800	0.013936	0.2500000	0.1255200
CBE	12.01100	-0.034148	0.3500000	0.2761440
HBE	1.00800	0.007298	0.2500000	0.1255200
CBI	12.01100	0.004260	0.3500000	0.2761440
HBI	1.00800	0.001058	0.2500000	0.1255200

Table S9. Bond stretching parameters for Noria-OEt.

Bond type	b_0 (nm)	K_0 (kJ mol^{-1}nm^{-2})
CBN-CBE	0.15290	224262.4
CBE-CBI	0.15290	224262.4
CBN-CRB	0.15100	265265.6
CRB-CRT	0.14000	392459.2
CRT-CRE	0.14000	392459.2
CRE-CRO	0.14000	392459.2
CRE-CRO	0.14000	392459.2
CRO-CRB	0.14000	392459.2
CRB-CRI	0.14000	392459.2
CRO-OH	0.13640	376560.0
CRT-OT	0.13640	376560.0
OT-CT	0.14100	267776.0
CT-CM	0.15290	224262.4
CBN-HBN	0.10900	284512.0
CBE-HBE	0.10900	284512.0
CBI-HBI	0.10900	284512.0
CRI-HRI	0.10800	307105.6
OH-HO	0.09450	462750.4
CRE-HRE	0.10800	307105.6
CT-HT	0.10900	284512.0
CM-HM	0.10900	284512.0

Table S10. Angle potential parameters for Noria-OEt.

Angle type	ϑ_0 (deg)	K_ϑ (kJ mol^{-1}rad^{-2})
CBE-CBN-HBN	107.800	276.144
CBN-CBE-HBE	107.800	276.144
CBN-CBE-CBI	112.700	488.273
CBE-CBI-CBE	112.700	488.273
CBE-CBI-HBI	107.800	276.144
CBI-CBE-HBE	107.800	276.144
CBE-CBN-HBN	107.800	276.144
CRB-CBN-CBE	114.000	527.184
CRT-CRB-CBN	120.000	585.760
CRI-CRB-CBN	120.000	585.760
CRB-CRI-HRI	120.000	292.880
CRB-CRT-OT	120.000	585.760
CRT-OR-CT	111.000	627.600
HT-CT-OT	109.500	292.880
HT-CT-CM	107.800	276.144
CT-CM-HM	107.800	276.144
CRI-CRB-CRO	120.000	527.184
CRB-CRO-OH	120.000	585.760
CRO-OH-HO	113.000	292.880
CRO-CRE-HRE	120.000	292.880
CRE-CRT-OT	120.000	585.760
CRT-CRE-HRE	120.000	292.880

Table S11. Dihedral potential parameters for Noria-OEt. Additionally, improper dihedrals were applied to aromatic rings using $\xi_0 = 180°$ and $k_\xi = 4.60240$ kJ/mol/rad^2.

Dihedral Type	$C1$(kJ mol^{-1})	$C12$(kJ mol^{-1})	$C3$(kJ mol^{-1})	$C4$(kJ mol^{-1})
HBN-CBN-CBE-HBE	0.62760	1.88280	0.00000	-2.51040
CBI-CBE-CBN-HBN	0.62760	1.88280	0.00000	-2.51040
CBN-CBE-CBI-HBI	0.62760	1.88280	0.00000	-2.51040
CBN-CBE-CBI-CBE	2.92880	-1.46440	0.20920	-1.67360
CBE-CBI-CBE-HBE	0.62760	1.88280	0.00000	-2.51040
CRI-CRB-CBN-HBN	30.33400	0.00000	-30.33400	0.00000
CRT-CRB-CBN-HBN	30.33400	0.00000	-30.33400	0.00000
CBN-CRB-CRI-HRI	30.33400	0.00000	-30.33400	0.00000
CBN-CRB-CRT-CRE	30.33400	0.00000	-30.33400	0.00000
CBN-CRB-CRI-CRB	30.33400	0.00000	-30.33400	0.00000
CRB-CRT-OT-CT	12.55200	0.00000	-12.55200	0.00000
CRB-CRT-CRE-HRE	30.33400	0.00000	-30.33400	0.00000
CRB-CRT-CRE-CRO	30.33400	0.00000	-30.33400	0.00000
CRB-CRI-CRB-CRO	30.33400	0.00000	-30.33400	0.00000
CRI-CRB-CRO-CRE	30.33400	0.00000	-30.33400	0.00000
CRI-CRB-CRO-OH	30.33400	0.00000	-30.33400	0.00000
CRB-CRO-OH-HO	7.03749	0.00000	-7.03749	0.00000
CRB-CRO-CRE-HRE	30.33400	0.00000	-30.33400	0.00000
CRB-CRO-CRE-CRT	30.33400	0.00000	-30.33400	0.00000
CRO-CRE-CRT-OT	30.33400	0.00000	-30.33400	0.00000
CRE-CRT-OT-CT	12.55200	0.00000	-12.55200	0.00000
CRB-CRT-OT-CT	12.55200	0.00000	-12.55200	0.00000
CRE-CRT-CRB-CBN	30.33400	0.00000	-30.33400	0.00000
CRT-OT-CT-CM	1.71544	2.84512	1.04600	-5.60656
CRT-OT-CT-HT	1.58992	4.76976	0.00000	-6.35968
HM-CM-CT-OT	0.97905	2.93716	0.00000	-3.91622

Table S12. Atom types, point charges and Lennard-Jones parameters for 15-crown-5.

Atom type	Mass	Charge (e)	Sigma (nm)	Epsilon (kj/mol)
HE	1.00800	-0.001572	0.2500000	0.1255200
CE	12.01100	0.189785	0.3500000	0.2761440
OE	15.99940	-0.373282	0.2900000	0.5857600

Table S13. Bond-stretching parameters for 15-crown-5.

Bond type	b_0 (nm)	K_0 (kJ mol^{-1}nm^{-2})
CE-HE	0.10900	284512.0
CE-CE	0.15290	224262.4
CE-OE	0.14100	267776.0

Table S14. Angle potential parameters for 15-crown-5.

Angle type	ϑ_0 (deg)	K_ϑ (kJ mol^{-1}rad^{-2})
HE-CE-HE	107.800	276.144
CE-CE-HE	110.700	313.800
HE-CE-OE	109.500	292.880
CE-OE-CE	109.500	502.080
CE-CE-OE	109.500	418.400

Table S15. Dihedral potential parameters for 15-crown-5.

Dihedral Type	$C1$(kJ mol^{-1})	$C12$(kJ mol^{-1})	$C3$(kJ mol^{-1})	$C4$(kJ mol^{-1})
HE-CE-CE-HE	0.62760	1.88280	0.00000	-2.51040
HE-CE-CE-OE	0.97905	2.93716	0.00000	-3.91622
CE-CE-OE-CE	1.71544	2.84512	1.04600	-5.60656
CE-OE-CE-HE	1.58992	4.76976	0.00000	-6.35968
OE-CE-CE-OE	-1.15060	1.15060	0.00000	0.00000

Table S16. Atom types, point charges and Lennard-Jones parameters for methane.

Atom type	Mass	Charge (e)	Sigma (nm)	Epsilon (kj/mol)
CMT	12.01100	-0.576308	0.3500000	0.2761440
HMT	1.00800	0.144077	0.2500000	0.1255200

Table S17. Bond-stretching parameters for methane.

Bond type	b_0 (nm)	K_0 (kJ mol^{-1}nm^{-2})
CMT-HMT	0.10900	284512.0

Table S18. Angle parameters for methane.

Angle type	ϑ_0 (deg)	K_ϑ (kJ mol^{-1}rad^{-2})
HMT-CMT-HMT	07.800	276.144

Table S19. Non-bonded parameters for correcting Noria-OEt and methane interactions.

Pair Type	b_0 (nm)	K_0 (kJ mol^{-1}nm^{-2})
CRI-CMT	0.352491	0.463554
CRI-HMT	0.297909	0.312528
HRI-CMT	0.291033	0.303467
HRI-HMT	0.245967	0.204598
CBE-CMT	0.350000	0.450115
CBE-HMT	0.295804	0.303467
HBE-CMT	0.295804	0.303467
HBE-HMT	0.250000	0.204598

S5.1 Computational methods

We conducted Molecular Dynamics (MD) simulations of three liquids: a 15-crown-5 neat liquid, a PL comprising Noria-OEt cages dissolved in 15-crown-5 at a 1:206 molar ratio, and the same PL loaded with methane molecules. The neat solvent consisted of 1000 15-crown-5 molecules enclosed in a cubic and periodic simulation box. For the PL, we selected the isomer of Noria-OEt with twelve ethyl groups over O sites symmetrical distributed and built a system made of 10 cages and 2060 solvent molecules (see **Figure S42**). Our simulations did not extend to the R3 isomer due to its strong resemblance to Noria-OEt in terms of intrinsic cavity radius and the formation energies of methane and 15-crown-5 inclusion complexes (**Table S20**). We believe that simulations of a liquid comprising either host or a mixture thereof are equally descriptive of the properties most relevant to our analysis: porosity, solvent exclusion and methane affinity.

Table S20: Comparison between characteristics of the Noria-OEt and R3 isomer hosts. The formation energies correspond to the inclusion of a methane or a 15-crown-5 (CET) molecule inside the intrinsic cavity of the either host. These energies were calculated using DFT at 0 K in vacuum following the specifications provided in section S5.4.

Characteristics	Noria-OEt	R3 isomer
Intrinsic cavity radius [nm]	0.226	0.223
CET inclusion energy [kcal/mol]	90.96	88.25
CH_4 inclusion energy [kcal/mol]	-7.05	-7.44

Before building the systems, we performed atomistic optimisations of all molecules using the *CP2K* software.[5] These calculations employed the density functional theory (DFT) method within the generalised gradient approximation. As exchange-correlation functional we used Perdew-Burke-Ernzerhof (PBE),[6] with Grimme's D2 dispersion correction,[7,8] Goedecker-Teter-Hutter pseudopotentials,[9] and the DZVP basis set. We calculated the electronic density using a 450 Ry cut-off, a 50 Ry rel cut-off and an accuracy of 10^{-5} Ry. We applied the RESP method in *CP2K* to obtain partial atomic charges from the optimized molecular structures. MD simulations were conducted with *Gromacs-2019.3*,[10] using an empirical force-field developed on the basis of the OPLS-AA force-field.[11] Trajectories were visualised with *Vmd v1.9*.[12] The file plconfig.gro contains a configuration of the PL phase equilibrated at 350 K and 1 bar.

Initial configurations of the PL were generated as follows: a) molecules were set at random places of a sufficiently large cubic box and heated from 1 to 300 K in NVT conditions; b) subsequently, the system was submitted to equilibration for 20 ns under the NPT ensemble at 300 K and 1 atm; c) the same conditions of the equilibration run were applied to a production stage that spanned 100 ns; d) the final configuration was annealed to 350 K for 10 ns and equilibrated at 350 K for 20 ns under NPT conditions; e) a final production run, lasting 100 ns, was conducted using the same simulation parameters. In all instances, we selected an integration timestep of 1 fs and set Nosé-Hoover as the thermostat with τ coupling constant of 0.1 ps. NPT instances employed the Parrinello-Rahman barostat with τ and compressibility set to 0.5 ps and 4 x 10^{-5} bar^{-1} respectively. Cut-offs for short- and long-range interactions were set to 1.4 nm. Lennard-Jones potentials were calculated with a force-shifting procedure, where energy and force contributions fall to zero smoothly for distances approaching the long-range cut-off. Coulomb forces were computed with the Particle Mesh Ewald

(PME) method. As a control parameter, we calculated the relative difference between the average density of each system and a reference experimental value. As shown in **Table S21**, relative differences in densities were below 3% in all cases.

Table S21. Average densities obtained from MD simulations of the neat solvent and PL at 300 and 350 K and 1 atm, under the NPT ensemble. The relative difference of these densities was calculated from experimental reference values: 1.113 g/mL for the neat solvent and 1.12 g/mL for the PL under normal temperature and pressure conditions.

System	Temperature (K)	Density (g/mL)	Relative difference
Neat solvent	300	1086.6	2,4%
	350	1037.7	-
PL	300	1089.2	2,8%
	350	1040.7	-

S5.2 Model of mdp file for *Gromacs* runs

```
; Run control
integrator = md
dt         = 0.001
comm-mode  = linear

; Output
nsteps         = 120000000
nstxout        = 10000
nstvout        = 10000
nstfout        = 10000
nstlog         = 10000
nstenergy  = 5000

; Neighbor searching
cutoff-scheme    = verlet
nstlist          = 1
ns-type          = grid
pbc        = xyz
rlist      = 1.4

; Electrostatics
coulombtype      = pme
rcoulomb    = 1.4

; Van den Waals
vdwtype     = cut-off
rvdw        = 1.4

; Ewald
fourier-nx = 15
fourier-ny = 15
fourier-nz = 15
pme-order  = 4
ewald-rtol = 1e-5
ewald-geometry = 3d

; Temperature coupling
tcoupl           = nose-hoover
tc-grps          = system
tau-t      = 0.1
```

```
ref-t       = 350.0

; Pressure coupling
pcoupl          = parrinello-rahman
pcoupltype = isotropic
tau_p       = 0.5
ref_p       = 1.01325
compressibility = 4e-5

; Velocity generation
gen-vel         = no

; Bonds
constraints      = hbonds
constraint_algorithm = lincs
lincs_order      = 4
lincs_iter = 1
morse       = no
```

S5.3 Free energy calculations

For free energy calculations, a number of Umbrella Sampling (US)[13] windows were simulated using *Gromacs-2019.1* for: the inclusion of a 15-crown-5 molecule inside a Noria-OEt in vacuum (a), the inclusion of a methane molecule inside a Noria-OEt host both in vacuum (b) and solution (c), and the insertion of a methane molecule inside a 15-crown-5 slab in vacuum. Potential of Mean Force (PMF) landscapes were calculated with the Weighted Histogram Analysis Method (WHAM)[14,15] using the WHAM package from *Gromacs*. For each PMF, error bars were obtained from 100 bootstrapped trajectories[16,17], with autocorrelation times integrated by the package.

For the inclusion complexes (a) (b) and (c), the free energy profiles were calculated using a reaction coordinate ξ defined as the distance between the centres of mass of the host and the guest. The restraining or biasing potential followed the form $V(\xi) = 0.5K(\xi-\xi_0)^2$, with an arbitrary constant K set to obtain an adequate overlapping of US histograms. The term $2k_BT \ln(\xi)$, where k_B represents the Boltzmann constant and T the absolute temperature, was added to the PMF profile as an entropic correction that arises from the definition of ξ[18]. Simulations under vacuum conditions, namely (a) and (b), were performed under NVT conditions at 350 K in cubic simulation boxes of 20 and 10 nm respectively. System (c) corresponded to the NPT ensemble at 350 K and 1 atm and contained 341 solvent molecules. The number, spread and simulation span of the US windows, as well as the values of K, are detailed in **Tables S22**, **S23** and **S24**.

For the PMF of the slab system (d) (**Figure S44**), ξ was defined as the distance along the z axis between the centres of mass of the methane molecule and the 15-crown-5 ether slab. As in prior instances, the biasing potential was $V(\xi) = 0.5K(\xi-\xi_0)^2$, but no entropic correction was applied to the resulting PMF since ξ coincides with a single cartesian coordinate component (z). Simulations were conducted in the NVT ensemble at 350 K using a simulation box of 4x4x12 nm³. The slab comprised 200 solvent molecules, with an average thickness of ~4 nm. The characteristics of the US windows are listed in **Table S25**.

Table S22. Umbrella Sampling parameters for the PMF of insertion of one solvent molecule in one Noria-OEt cage in vacuum at 350 K.

Range (nm)	N° of windows	Window spacing (nm)	Simulation length (ns)	K (kJ mol⁻¹ nm⁻²)

0.0 to 0.5	50	0.01	5	10000
0.5 to 1.0	50	0.01	5	5000
1.0 to 2.0	25	0.04	10	2000
2.0 to 5.0	75	0.04	5	500

Table S23. Umbrella Sampling parameters for the PMF of insertion of one solvent molecule in one Noria-OEt cage in vacuum at 350 K.

Range (nm)	N° of windows	Window spacing (nm)	Simulation length (ns)	K (kJ mol^{-1} nm^{-2})
0.0 to 4.5	46	0.10	10	500

Table S24. Umbrella Sampling parameters for the PMF of insertion of one solvent molecule in one Noria-OEt cage in solution at 350 K and 1 atm.

Range (nm)	N° of windows	Window spacing (nm)	Simulation length (ns)	K (kJ mol^{-1} nm^{-2})
0.0 to 4.0	41	0.10	10	2000

Table S25. Umbrella Sampling parameters for the PMF of introduction of one methane in a 15-crown-5 slab in vacuum at 350 K.

Range (nm)	N° of windows	Window spacing (nm)	Simulation length (ns)	K (kJ mol^{-1} nm^{-2})
0.0 to 4.0	41	0.10	10	1000
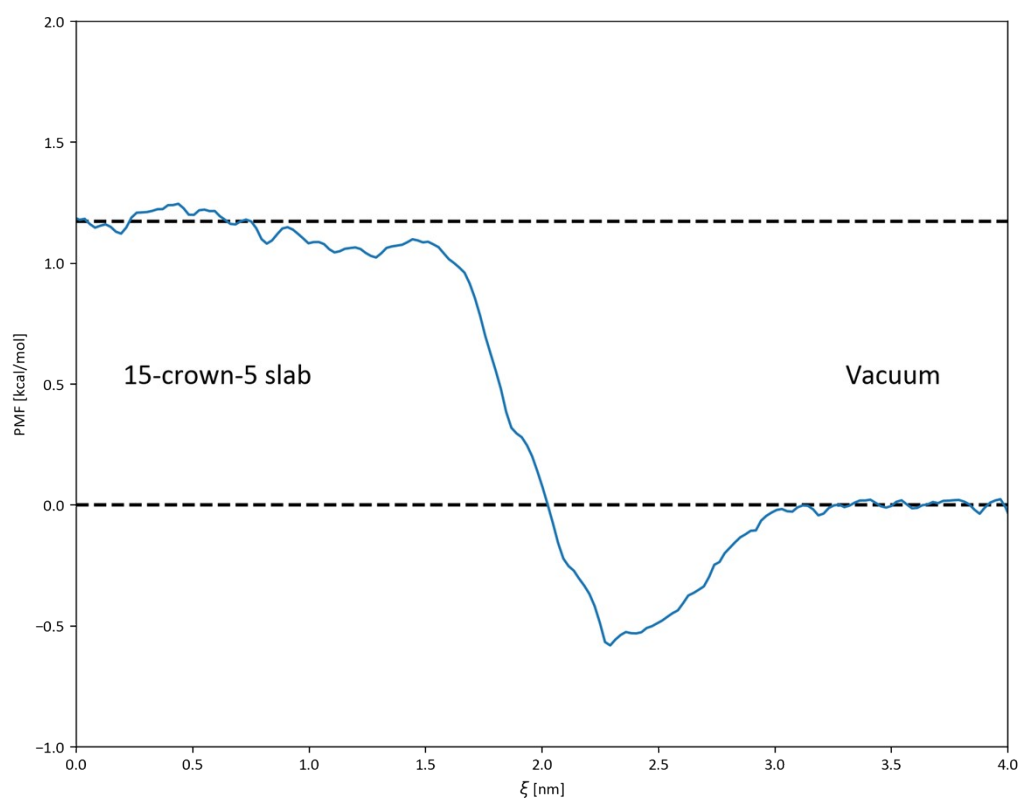
Figure S44. Potential of Mean Force (PMF) computed by Umbrella Sampling for the insertion of a methane molecule in 15-crown-5 slab in vacuum at 350 K. The reaction coordinate ξ corresponds to the distance between the centres of mass of the slab and the gas molecule. Notice that the minimum PMF occurs when the methane molecule reaches the surface of the liquid slab. The total free energy cost for inserting (solvating) a single methane molecule from vacuum into 15-crown-5 is 1.17 kcal/mol.

S5.4 Formation energies

Non-bonded interactions between methane atoms and key Noria-OEt atoms were adjusted in the force-field to correctly reproduce the formation energies from DFT results (**Table S19**). The DFT methods used to calculate these values (**Table S26**) are described in the Computational methods section. In order to obtain MM formation energies, all DFT-optimized geometries were subjected to further optimization using the steepest descent and conjugated gradient algorithms implemented in *Gromacs*.

Table S26. Formation energies of inclusion complexes obtained from Density Functional Theory (DFT) and Molecular Mechanics (MM) calculations performed with the *CP2K* and *Gromacs* programs, respectively. Energies computed for geometry-optimized isolated molecules (gas phase calculations) at 0 K. Inclusion complex variants are illustrated in **Figure S45**.

Inclusion complex	DFT Formation Energy (kcal/mol)	MM Formation Energy (kcal/mol)
Noria-OEt-solvent	90.96	109.91
Noria-OEt-methane (inside)	-7.05	-7.05
Noria-OEt-methane (outside)	-6.79	-6.11
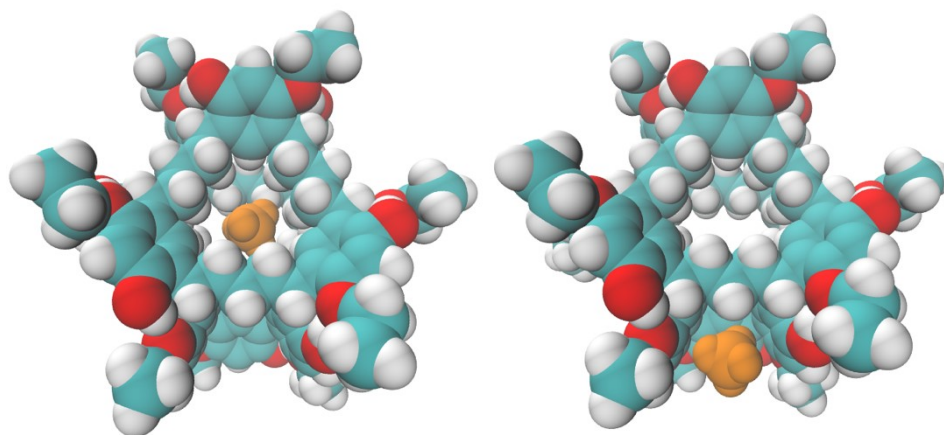
Figure S45. Top perspective of two Noria-OEt-methane inclusion complexes where the methane molecule (orange) is located either inside the intrinsic cavity (left) or in one of the six outer indentations (right). The corresponding formation energies are listed in **Table S26**.

S5.5 Cavity size distributions and relative porosity

In order to quantify the effective porosity of the PL relative to the neat solvent, we calculated the insertion probability p(R) of a rigid sphere of radius R in an arbitrary point of each liquid phase.[19,20] This probability is given by:

$$p(R) = \langle V_R \rangle / V$$

where $\langle V_R \rangle$ represents the average volume accessible to a spherical solute of radius R, and V the volume of the liquid sample. Alternatively, p(R) can be expressed in terms of $p_m(R)$, the probability that R is the radius of the largest sphere that can be inserted in an arbitrary point of the liquid, as follows:

$$p(R) = \int_R^\infty p_m(R')dR'$$

We defined the relative porosity of the PL, W(R), as the quotient between the insertion probability in the PL and in the neat solvent at the same temperature and pressure. For each of these, p(R) was obtained by creating a grid along the x, y and z axes of the simulation cells, each point set 0.1 nm apart along the axes. We calculated the radii of the largest spheres that could be inserted at each grid point without overlapping with any atomic van der Waals radius.

S5.6 Mean square displacement

Figures S46.a and **S46.b** show the mean square displacement (MSD) of a) 15-crown-5 (CET) and b) Noria-OEt molecules for different systems at 350 K. These systems were a PL loaded with methane at 1 bar, another PL loaded with methane at 5 bar, and a neat CET liquid at 1 bar. CET diffusion was linear throughout the simulations and similar for all systems analysed. The difference between diffusion coefficients, D, for the PL and neat solvent at 1 bar was approximately 6%, which illustrates that the low concentration of Noria-OEt had no significant effect on solvent diffusion. Unlike CET, the linear regime in Noria-OEt diffusion was brief, spanning the interval between 40 and 70 ns. As expected from the difference in size between both molecule types, Noria-OEt diffusion was roughly seven times slower than that of CET.
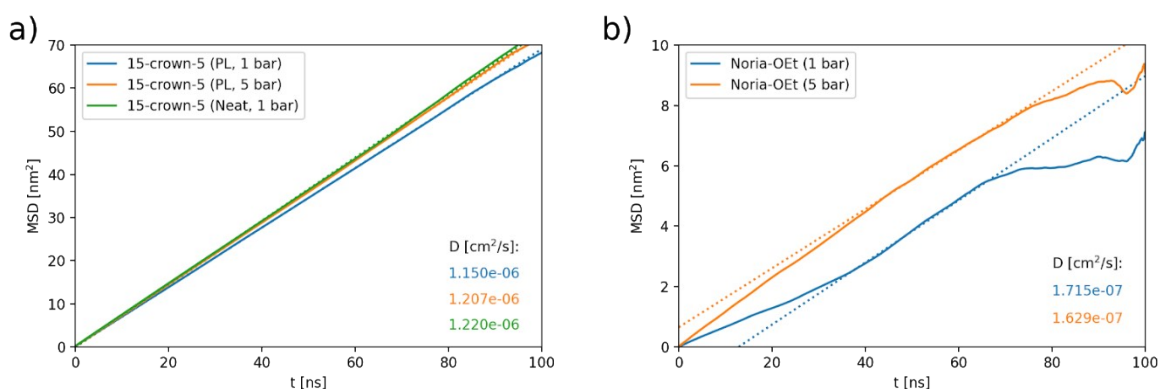
Figure S46. Mean square displacement (MSD) of a) 15-crown-5 (CET) and b) Noria-OEt (Noria) molecules for: a PL loaded with methane at 1 bar, a PL loaded with methane at 5 bar, and a neat CET liquid. Diffusion coefficients, D, shown in the bottom-right corner on each figure, correspond to the least-square linear fitting to intervals a) 10 to 90 ns and b) 40 to 70 ns.

S6. Crystal Data and Experimental

S6.1 X-ray crystallography

Crystal Data for Noria. $C_{143}H_{224}O_{47}$, M_r = 2695.21, trigonal, R-3 (No. 148), a = 30.9611(2) Å, b = 30.9611(2) Å, c = 13.12040(10) Å, α = 90°, β = 90°, γ = 120°, V = 10892.06(16) Å^3, T = 100(2) K, Z = 3, Z' = 0.166667, μ(Mo K$_\alpha$) = 0.091 mm^{-1}, 178473 reflections measured, 6248 unique (R_{int} = 0.0244) which were used in all calculations. The final wR_2 was 0.1889 (all data) and R_1 was 0.0631 (I≥2 σ(I)).

Crystal Data for R3. $C_{114}H_{132}O_{30}S_6$, M_r = 2174.55, triclinic, P-1 (No. 2), a = 19.5728(5) Å, b = 22.2124(7) Å, c = 22.5739(6) Å, α = 117.141(3)°, β = 115.302(3)°, γ = 90.835(2)°, V = 7623.2(4) Å^3, T = 100(2) K, Z = 2, Z' = 1, μ(Mo K$_\alpha$) = 0.146 mm^{-1}, 110888 reflections measured, 26905 unique (R_{int} = 0.0879) which were used in all calculations. The final wR_2 was 0.2796 (all data) and R_1 was 0.0894 (I≥2 σ(I)).

S6.2 Data collection and processing

Suitable crystals were selected, and data collected following a standard method, [21] on a Rigaku FRE+ diffractometer equipped with VHF Varimax confocal mirrors and an AFC12 goniometer and HyPix 6000 detector, equipped with an Oxford Cryosystems low-temperature device operating at T = 100(2) K. Cell determination, data collection, data reduction, cell refinement and absorption correction were carried out using CrysAlisPro.[22] The structures were solved with the ShelXT[23] structure solution program using the Intrinsic Phasing solution method and by using Olex2[24] as the graphical interface. The models were refined with version 2018/3 of ShelXL[25] using Least Squares minimisation.

CCDC 2080523 and 2080524 contains supplementary X-ray crystallographic data for **Noria** and **R3** respectively. This data can be obtained free of charge via http://www.ccdc.cam.ac.uk/conts/retrieving.html, or from the Cambridge Crystallographic Data Centre, Union Road, Cambridge, CB2 1EZ; fax(+44) 1223-336-033 or email: deposit@ccdc.cam.ac.uk.

S6.3 Noria Single Crystal
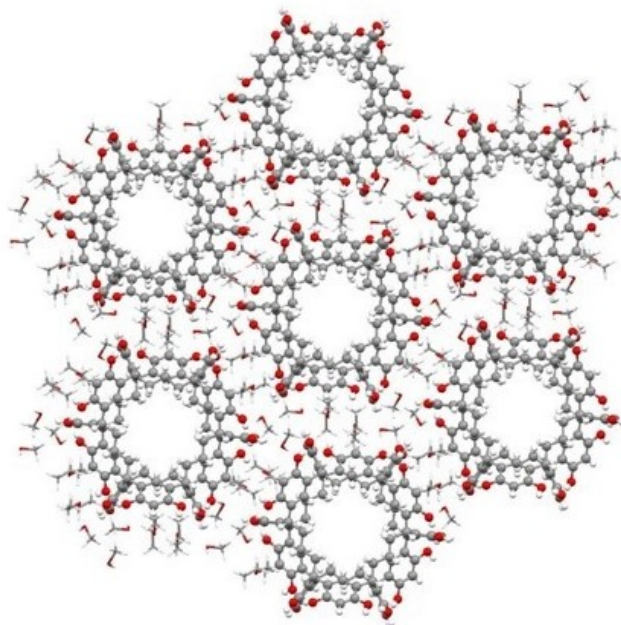
Figure S47. Hexagonal packing arrangement of Noria single crystals.

S7.1 R3 Single Crystal
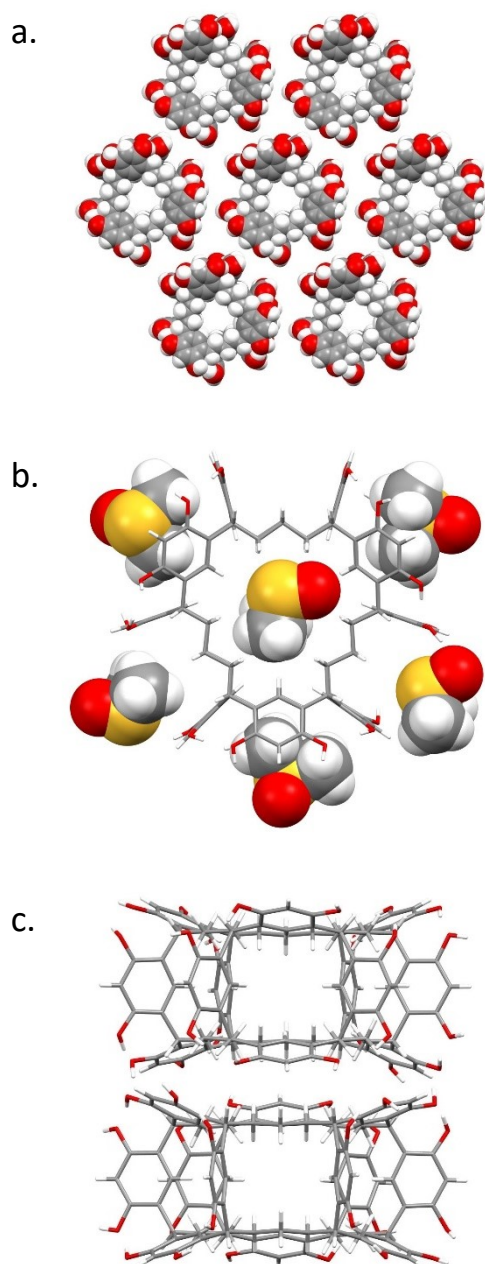
Figure S48. a. Hexagonal packing arrangement of R3 single crystals, **b.** Arrangement of DMSO solvent molecules in a R3 single crystal, **c.** Dimers of R3.

S7. References

1. a) H. Kudo, R. Hayashi, K. Mitani, T. Yokozawa, N. C. Kasuga and T. Nishikubo, *Angew. Chemie Int. Ed.*, 2006, **45**, 7948–7952. b) H. Kudo, Y. Suyama, H. Oizumi, T. Itani and T. Nishikubo, *J. Mater. Chem.*, 2010, **20**, 4445–4450.

2. a) N. Niina, H. Kudo, T. Nishikubo, *Chem. Lett.* 2009, **38**, 1198–1199. b) N. Niina, H. Kudo, K. Maruyama, T. Kai, T. Shimokawa, H. Oizumi, T. Itani and T. Nishikubo, *Polym. J.*, 2011, **43**, 407–413.

3. D. Shimoyama, R. Sekiya, H. Maekawa, H. Kudo, T. Haino, *CrystEngComm.*, 2020, **22**, 4740–4747.

4. J. Cahir, M. Y. Tsang, B. Lai, D. Hughes, M. A. Alam, J. Jacquemin, D. Rooney and S. L. James, *Chem. Sci.*, 2020, **11**, 2077–2084.

5. J. Hutter, M. Iannuzzi, F. Schiffmann, J. VandeVondele, *WIREs Comput. Mol. Sci.* 2014, **4**, 15–25.

6. J. P. Perdew, K. Burke, M. Ernzerhof, *Phys. Rev. Lett.* 1996, **77**, 3865–3868.

7. S. Grimme, *J. Comput. Chem.* 2006, **27**, 1787–1799.

8. S. Grimme, J. Antony, S. Ehrlich and H. Krieg, *J. Chem. Phys.*, 2010, **132**, 154104.

9. S. Goedecker, M. Teter, J. Hutter, *Phys. Rev. B*. **1996**, 54, 1703–1710.

10. M. J. Abraham, T. Murtola, R. Schulz, S. Páll, J. C. Smith, B. Hess and E. Lindahl, *SoftwareX*, 2015, **1**–**2**, 19–25.

11. W. L. Jorgensen, D. S. Maxwell and J. Tirado-Rives, *J. Am. Chem. Soc.*, 1996, **118**, 11225–11236.

12. W. Humphrey, A. Dalke and K. Schulten, *J. Mol. Graph.*, 1996, **14**, 33–38.

13. D. Frenkel and B. Smit, Understanding molecular simulation, Academic Press, Inc., 2nd edn, 2001.

14. B. Roux, *Comput. Phys. Commun.*, 1995, **91**, 275–282.

15. S. Kumar, J. M. Rosenberg, D. Bouzida, R. H. Swendsen and P. A. Kollman, *J. Comput. Chem.*, 1995, **16**, 1339–1350.

16. B. Efron, *Ann. Stat.*, 1979, **7**, 1–26.

17. J. S. Hub, B. L. de Groot and D. van der Spoel, *J. Chem. Theory Comput.*, 2010, **6**, 3713–3720.

18. D. Trzesniak, A.-P. E. Kunz and W. F. van Gunsteren, *ChemPhysChem*, 2007, **8**, 162–169.

19. A. Pohorille and L. R. Pratt, *J. Am. Chem. Soc.*, 1990, **112**, 5066–5074.

20. L. R. Pratt and A. Pohorille, *Proc. Natl. Acad. Sci.*, 1992, **89**, 2995–2999.

21. S. J. Coles and P. A. Gale, *Chem. Sci.*, 2012, **3**, 683–689.

22. CrysAlisPro Software System, Rigaku Oxford Diffraction, **2021**.

23. G. M. Sheldrick, *Acta Crystallogr. Sect. A*, 2015, **71**, 3–8.

24. O. V Dolomanov, L. J. Bourhis, R. J. Gildea, J. A. K. Howard and H. Puschmann, *J. Appl. Cryst.*, 2009, **42**, 339–341.

25. G. M. Sheldrick, *Acta Cryst*. Sect. C, 2015, **C72**, 3–8.